NASA CONTRACTOR REPORT

NASA CR-1794

PENETRATION AND SPREADING OF TRANSVERSE JETS OF HYDROGEN IN A MACH 2.72 AIRSTREAM

by John P. Wagner, James M. Cameron, and Frederick S. Billig

Prepared by
THE JOHNS HOPKINS UNIVERSITY, APPLIED PHYSICS LABORATORY
Silver Spring, Md. 20910
for

NATIONAL AERONAUTICS AND SPACE ADMINISTRATION • WASHINGTON, D. C. • MARCH 1971

1. Report No.	2. Government Accession No.	3. Recipient's Catalog No.
NASA CR-1794		

4. Title and Subtitle	5. Report Date
PENETRATION AND SPREADING OF TRANSVERSE JETS OF HYDROGEN IN A MACH 2.72 AIRSTREAM	March 1971
	6. Performing Organization Code
7. Author(s)	8. Performing Organization Report No.
John P. Wagner, James M. Cameron and Frederick S. Billig	
	10. Work Unit No.
9. Performing Organization Name and Address	
The Johns Hopkins University, Applied Physics Laboratory 8621 Georgia Avenue Silver Spring, Maryland 20910	11. Contract or Grant No. NASR-76
	13. Type of Report and Period Covered
12. Sponsoring Agency Name and Address	Contractor's Report
National Aeronautics and Space Administration Washington, D.C. 20546	14. Sponsoring Agency Code

15. Supplementary Notes

16. Abstract

Hydrogen was injected from a flat-plate model (simulating the wall of a supersonic combustor) into a Mach 2.72 air stream. The transverse, sonic, underexpanded-jet injection was either from a single port or from a five-port injector having the same total throat (exit) area, with a 3-diameter center-to-center spacing. The latter injector was tested with the row of ports either aligned with or perpendicular to the mainstream flow direction. Schlieren photographs, cone-static and pitot pressure surveys, and gas-sampling surveys were used to define in detail the complex flow field. In the y-z (normal) plane at the downstream (x) station 5 equivalent-single-port diameters (d_{je}) from the injector, the effective cross-sectional area of fuel distribution achieved with the aligned multiport injector was ~ 22% greater than that for the perpendicular multiport injector and ~ 7% greater than that for the single port.

17. Key Words (Suggested by Author(s))	18. Distribution Statement
Scramjet technology Jet penetration and jet spreading Supersonic mixing	Unclassified - Unlimited

19. Security Classif. (of this report)	20. Security Classif. (of this page)	21. No. of Pages	22. Price*
Unclassified	Unclassified	44	$ 3.00

*For sale by the National Technical Information Service, Springfield, Virginia 22151

PENETRATION AND SPREADING OF TRANSVERSE JETS OF HYDROGEN IN A MACH 2.72 AIRSTREAM

By John P. Wagner, James M. Cameron,
and Frederick S. Billig
Applied Physics Laboratory, The Johns Hopkins University
Silver Spring, Maryland

SUMMARY

Hydrogen was injected from a flat-plate model (simulating the wall of a supersonic combustor) into a Mach 2.72 air stream. The transverse, sonic, underexpanded-jet injection was either from a single port or from a five-port injector having the same total throat (exit) area, with a 3-diameter center-to-center spacing. The latter injector was tested with the row of ports either aligned with or perpendicular to the mainstream flow direction. Schlieren photographs, cone-static and pitot pressure surveys, and gas-sampling surveys were used to define the complex flow field in the y-z (normal) plane at the downstream (x) station 5 equivalent-single-port diameters (d_{je}) from the injector. For the single-port injector itself, data also were obtained at $x/d_{je} = 10$.

Deduced y-z contours for static pressure and temperature, Mach number, local velocity, mass flux of the H_2-air mixture, H_2 mass flux, and total pressure are presented. The H_2 mass flux distribution was integrated graphically to obtain a total H_2 flow rate for comparison with the metered incoming value (i.e., an H_2 mass balance). The former (deduced) rate at $x/d_{je} = 5$ was lower than the latter (metered) rate for all three injectors: 4% low for the single-port injector, 12% low for the multiport, perpendicular, and 10% low for the multiport, aligned. In view of the large number of measurements and data manipulations involved in these balances, the results are sufficiently good to confirm the general validity of these techniques.

Performances of the injectors are compared on the basis of a) the mass-averaged total pressure recovery at $x/d_{je} = 5$ for the air needed for a stoichiometric mixture, and b) the achieved fuel distribution. The aligned multiport injector and the single port injector both gave estimated equivalent air total pressure recoveries near 71%, whereas the perpendicular multiport injector gave the considerably poorer value of 61%. These estimated pressure recoveries were obtained by mass-averaging properties for two flow regions, assuming that those two flows then mixed in a constant-area streamtube, and determining the ratio of the total pressure of this uniformly mixed (and stoichiometric) flow to the total pressure of the undisturbed air stream ahead of the injector. The two flow regions (in the $x/d_{je} = 5$ plane) used for this calculation were 1) the

region bounded by the 0% H_2 concentration contour, and 2) the region just outside this contour which would provide sufficient additional air to make the resulting mixture stoichiometric overall.

At $x/d_{je} = 5$ the effective cross-sectional area of fuel distribution for the aligned multiport injector was $\sim$ 22% greater than that for the perpendicular multiport injector and 7% greater than that for the single port injector. With respect to vertical penetration per se, the perpendicular multiport injector was even poorer, giving only 30% as much penetration as the aligned injector in terms of the Mach disk height in the jet (last jet in the "stair-step" set in the aligned case), or 60% as much in terms of the H_2 concentration profiles at $x/d_{je} = 5$.

INTRODUCTION

Of the various possible ways of injecting fuel into the supersonic combustor of a scramjet engine, one of the more attractive methods is injection from flush ports in the combustor wall. This approach, which avoids placement of any fuel injection hardware in the severe environment of the combustor flow field, has been under study for several years. Its advantages are simplicity and structural reliability. Its chief disadvantage is the limited degree to which a transverse fuel jet from a wall can penetrate the supersonic air stream. For this reason, the question of interaction between adjacent fuel jets is of interest, i.e.: Will certain arrangements of ports improve penetration for a given mass flow of fuel? The experimental study reported herein has addressed this question with respect to two simple multiport arrangements: five ports in a row in the air stream direction, and the same five-port injector rotated 90° in its flush wall installation so that the ports are abreast of each other. The former case will be called the "aligned" orientation; the latter, the "perpendicular" or "cross-flow" orientation. Results are compared with results for a single-port injector having the same total throat flow area.

Prior work at the Applied Physics Laboratory on gaseous jet penetration from single ports, both circular and elongated, has been reported in Refs. 1-4. The most recent analytical work has been reported briefly in Ref. 5. Recent work done at other laboratories is reported in Refs. 6-8. Suffice it to say here that a rather complete understanding of the important near-downstream flow field now exists for single-port injectors. A unified and internally consistent analytical treatment for the jet penetration and jet structure has been developed (Ref. 5).

The present report emphasizes the evaluation of experimental results. No attempt has yet been made to extend the aforementioned analytical model to include interaction effects between adjacent fuel jets. However, to provide a rather complete experimental picture, the flow field is characterized by contours of all flow properties at the downstream station, $x/d_{je} = 5$, where d_{je} is the diameter of the equivalent single port (in this case, 0.2 in.). All cases are for sonic injection

into a Mach 2.72 air stream. Comparisons of the penetration and flow field of the single hole injector and the five hole injector having a center-to-center spacing of 3 port diameters are made. For each injector, an approximate mixing analysis is used to estimate, from the deduced flow properties at $x/d_{je} = 5$, the total pressure loss that would be incurred to produce a completely mixed, stoichiometric fuel-air mixture. This loss is then further examined with respect to its distribution between jet interaction effects and mixing loss.

SYMBOLS

a	speed of sound
C_D	discharge coefficient
d_j^*	throat diameter of individual injector port (for the single port injector, $d_j^* = d_{je}$)
d_{je}	diameter of an equivalent single port having a throat area equal to the total throat area of a multiport injector (for all data reported herein, $d_{je} = 0.200$ in.)
ER	fuel/air equivalence ratio
g	acceleration of gravity = 32.17 ft/sec^2
ℓ	port center-to-center spacing
M	Mach number
$\mathfrak{m}$	molecular weight
p	static pressure
p_b	effective back pressure = $\frac{2}{3} p_{t'_a}$
$\overline{p}_t$	mass-averaged total pressure
$p_{t'}$	pitot pressure
q	$\rho u^2/2$ = dynamic pressure
R^o	universal gas constant = 1545.32 $ft\text{-}lb_f/lb_m\text{-}°R$
R_{mix}	gas constant of the mixture
T	temperature

u	axial velocity downstream from the injection plane
X	mole fraction
x	position downstream from the injector port
Y	mass fraction
y	normal distance from the plate surface
z	lateral distance from the centerline of the injector
γ	ratio of specific heats
ρ	density of air-hydrogen mixture
θ	cone half-angle

Subscripts:

a	undisturbed mainstream condition
c	cone surface conditions
i	i^{th} species
j	initial jet conditions
mix	properties of air-hydrogen mixture
o	center of Mach disk (normal shock in jet structure)
t	total conditions

Superscripts:

$( )'$	conditions following normal shock
$( )^*$	sonic conditions (injector throat; for the sonic injectors reported herein, this also is the injector port exit condition)

APPARATUS AND PROCEDURE

The experimental setup used in this study (Fig. 1) is similar to that of Orth and Funk (Ref. 2). Hydrogen was injected transversely from a flat plate injector at sonic conditions into a Mach 2.72 airstream. Two different types of injectors were used: a single (0.200-inch-diameter) circular port and a fuel injector insert made with five circular ports of 0.089-inch diameter (d_j^*) and a center-to-center spacing (ℓ) of 0.268 inch, so that $\ell/d_j^* = 3$.

In the initial tests with the single-port injector, the gas samples were obtained from a 7-probe rake. The 0.042-in.-O.D. probes were located at the corners and in the center of a hexagon, with a center-to-center spacing of 0.28 in. Samples were taken over a 10-second interval, withdrawn into bottles and analyzed by gas chromatography (Ref. 2). Runs were then repeated for different probe positions. Cone-static, pitot, and surface-static pressures were measured with a two-probe rake mounted on a mechanically operated traversing mechanism. For preselected values of x and y (Fig. 2), the rake was moved at a rate of 1 in./min in the z direction. Preliminary tests had established that the time response of the pressure measuring system was sufficiently rapid that readings obtained while traversing were identical to those with the probe in a stationary position.

The 0.125-in.-diameter cone-static probe had a 15° half-angle. Four separately ported, 0.015-in.-diameter static taps were located at 12, 3, 6 and 9 o'clock, 0.170 in. from the tip. The 0.18-in.-diameter, hemispherically nosed pitot-static probe had a 0.015-in.-diameter pitot tube and four 0.015-in.-diameter surface static ports located 0.522 in. from the probe tip. The probes were separated by 0.50 in. to assure that disturbances from the pitot probe would not affect the cone-static readings.

To decrease the number of test runs required to map the flow field for the 5-port injector, a seven-point pitot pressure rake, a redesigned 7-point gas-sampling rake, and a four-point cone-static rake were used. Runs were made with one of the rakes mounted in the previously mentioned traversing mechanism. Continuous traverses were made with the pressure rakes, and gas samples were obtained with three 10-second stops of the traverse device, giving a total of 21 samples per run. The rakes were arranged in a vertical alignment with 0.25-in. spacing of the pitot and gas-sampling probes and 0.50-in. spacing of the cone-static probes. The designs of the individual cone-static and gas-sampling probes were the same as used in the single-port injector tests. A 0.065-in.-diameter tube with 0.009-in. wall was used for the pitot probes, and the surface statics were eliminated because the results from the single-port tests showed that the region of the flow in which these measurements would be needed for data reduction was quite small.

Schlieren photographs for both series of tests were obtained with a focal-plane camera and recorded on ASA 3000 Polaroid film.

With the gas composition and total temperature defined (see Appendix), the combination of cone-static and pitot pressures is sufficient to define completely all other properties of the flow, as long as the flow is supersonic, the flow angularity is moderate, and the shock on the conical probe is attached. For the 15°-half angle probe used in these tests, detachment of the conical shock occurs at $M < 1.13$ for flow aligned with the probe axis. With four separately metered taps it is possible to determine the local flow angularity for moderate angles of attack if the probe diameter is small compared to the transverse gradient in Mach number (Ref. 9).

The pitot probe was designed to be insensitive to angles of attack $\leq 15°$ (Ref. 10). Thus, sufficient information was available to define the three-dimensional character of the flow field. However, the required analytical effort would have been excessive, relative to the small gain in understanding it would have provided. Instead, it was assumed that the flow was coaxial (i.e., parallel to the x axis) for $x/d_{je} \geq 5$, and the average values of the four static pressures were used, unless the deviations in the four readings were large, indicating either that the bow shock from an adjacent probe was causing a spurious effect or that the yaw angle of the flow was large. For the few points in which this occurred, either the high pressure was disregarded or the data were not included. Moreover, some difficulty was experienced in precisely determining the $z/d_j^* = 0$ plane, with the cone probe rake. To alleviate this problem, the data taken on both sides of the $z/d_j^* = 0$ plane were examined to find the plane of symmetry and the $z/d_j^* = 0$ point was adjusted accordingly.

In regions of the flow having $M \leq 1.13$ the pitot reading is essentially the total pressure (i.e., $p_t'/p_t = 0.998$ at $M = 1.13$; $p_t'/p_t = 1.00$, $M \leq 1$) and the second property used is static pressure. The static pressure can be obtained from the static taps on the pitot probe or from a smooth extrapolation of a curve of deduced static pressures for the regions of $M > 1.13$ to the flat plate surface pressure. As it turned out, the region of flow with $M < 1.13$ in these tests was so small that only the latter method was used.

EXPERIMENTAL RESULTS

A schematic of the test setup showing the axis system used is given in Fig. 2. To insure direct comparability of results, the critical parameters that control jet penetration (Ref. 1), jet total/effective back pressure, p_{t_j}/p_b, and momentum ratio, q_j/q_a, were closely matched for the two different injectors.

Single-Port Data

Tests were made with a 0.200-in.-diameter injector at $540 \leq p_{t_j} \leq 592$ psia and $356 \leq p_{t_a} \leq 360$ psia. Gas samples, pitot pressures, and cone-static pressures were obtained for both off-plate distances y/d_j^* and off-center distances (z/d_j^*) and two downstream axial locations $x/d_j^* = 5$ and 10. Results of the analysis of the gas samples are shown in Fig. 3. The contours of constant mole percentage of hydrogen were generated from crossplots of the discrete data points which are shown. The near circular shape of the contours is consistent with observations of Zukoski and Spaid (Ref. 11) and Torrence (Ref. 6) for argon injection into a Mach 2.56 airstream. The cone-static and pitot pressure data normalized to the air total pressure are shown in Figs. 4 and 5. The general trend of the pitot pressures is a monotonic increase with a fixed y/d_j^* and increasing z/d_j^*, or a fixed z/d_j^* and increasing y/d_j^*, with some exceptions, viz., the dip

in the curve for $x/d_j^* = 5$, $y/d_j^* = 3.125$ and the inversion of the curve at $x/d_j^* = 5$, for $y/d_j^* = 1.25$ and 0.625. Cone static pressures are less systematic.

Schlieren photographs from these tests and from numerous other tests were examined to locate the position of the Mach disk in the underexpanded secondary jets. The results, summarized in Ref. 5, show that the vertical distance to the center of the Mach disk can be approximated by the simple expression

$$y_o/d_j^* = (p_j^*/p_b)^{\frac{1}{2}} M_j^{\frac{1}{4}} \qquad (1)$$

For $p_{t_j}/p_b = 5.75$, $p_j^*/p_a = 3.04$, and $y_o/d_j^* = 1.74$. Reference 5 also gives a method for obtaining the downstream displacement of the center of the Mach disk, x_o, and for this case $x_o/d_j^* \simeq 2.04$. Although the additional penetration downstream of the Mach disk is significant, as evidenced in Figs. 3 (the maximum H_2 concentration which lies near the center of mass at $x/d_j^* = 5$ is at $y/d_j^* = 2.7$ and at $x/d_j^* = 10$ is at $y/d_j^* = 2.9$) this location is a good indicator of the ultimate penetration. Thus, one of the comparisons to be made between single and multiple hole injectors will be based on y_o/d_j^*.

Multiple Port Data

This section deals with the measurements made with the transverse injection of hydrogen from a row of 5 circular ports that were either aligned with or perpendicular to the Mach 2.72 airstream. The 0.089-in. diameter of the individual ports was selected so that the total cross-sectional area of the five ports would be equal to that of the 0.200-in.-diameter injector used in the single port tests. Thus, for the same airflow conditions, equal p_{t_j}'s would give equal mass flows, and direct comparisons could be made. The gas sampling and pressure measurements were made with $p_{t_j} \simeq 565$ psia to match the single port results. Some runs were also made in which p_{t_j} was varied from 200 to 693 psia, and schlieren pictures were taken to examine the structure of the underexpanded jets and to determine the Mach disk locations.

Concentration profiles at $x/d_{je} = 5$ (downstream distance is measured from the center of the third circular port) for the two configurations are compared in Fig. 6. Here d_{je} is the equivalent diameter for the total throat area of the five ports, and it is equal to d_j^* for the single-port injector, i.e., 0.200 in. The perpendicular injector has poor penetration characteristics, with an abrupt fall-off in hydrogen concentration from 50 mole % to 0 mole % in going from $y/d_{je} \simeq 2$ to $y/d_{je} = 3$ (i.e., from 0.4 in. to 0.6 in. from the plate). The aligned injector compares favorably in penetration and spreading with the single-port injector, but the concentration goes through a maximum with off-center distance,

whereas for the single-port injector it decreased monotonically from a maximum at $x/d_{je} = 0$, $y/d_{je} \simeq 3$.

The initial gas-sampling measurements for the aligned injector indicated the seemingly anomalous result of low concentration in the "core" region at $y/d_{je} = 3$, $z/d_{je} = 0$ and a peak concentration profile 1-2 d_{je} laterally from this point. This result was verified by taking additional gas samples (to a total of 42) in the region $0 \leq z/d_{je} \leq 1.5$, $0.625 \leq y/d_{je} \leq 5.625$. This characteristic should enhance the downstream mixing, but detailed numerical calculations of coaxial turbulent mixing must be made to verify this conclusion. In any event, the area enclosed by the zero-H_2 concentration profile is $\sim 7\%$ greater than with the single-port injector at equivalent testing conditions.

With the perpendicular injector the abrupt drop in concentration between $y/d_{je} = 2$ and $y/d_{je} = 3$ was noted. In this region only the point measurements are shown, and no attempt has been made to define the contours. The lateral spreading of the hydrogen is greater than with a single port, but the penetration is considerably less. Additional results at other hole spacings are being made in a follow-on program to determine the spacing at which the flow becomes two-dimensional rather than three-dimensional in character.

Figures 7 and 8 compare the cone-static and pitot pressure profiles for the two injector orientations at $x/d_{je} = 5$. The data for the aligned injector show trends similar to those for the single 0.200-in.-diameter port (Fig. 4). For the perpendicular orientation, the pressures vary only slightly with the lateral dimension, z/d_{je}, and represent a nearly two-dimensional flow field.

Typical schlieren photographs of the jet structure for the two orientations of the five-port injector are shown in Fig. 9. With the perpendicular orientation the flow field is similar to that of the transverse slot injector (Ref. 12, Fig. 6), i.e., it is characterized by large separated zones fore and aft of the hydrogen jet, and the Mach disk is nearly parallel to the plate. For the aligned injector an interesting shock pattern resembling an ascending staircase is observed. The structure of the most upstream jet is similar to the structure of the discharge from a single orifice. The secondary jet is partially bent in the downstream direction before the Mach disk is formed (see Fig. 4b, Ref. 5). The remaining jets appear to be shielded from the cross flow and are similar to the discharge into a quiescent medium (see Fig. 4a, Ref. 5). Each succeeding Mach disk has greater penetration indicating that the effective back pressure is decreasing in the downstream direction.

The Mach disk height y_o (i.e., the vertical dimension to the center of the Mach disk) serves as an indicator of relative penetration. Table 1 compares the measured, normalized Mach disk heights for the 5-port injector in the perpendicular orientation (y_o/d_j^*, where d_j^* is 0.089 in., the single hole diameter) with the single-port correlation, Eq. (1) [i.e.,

Table 1

Mach Disk Height for Five-Port Injector in Perpendicular Orientation

Jet Total Pressure p_{t_j}	Distance to Mach Disk y_o, in.	$\frac{y_o}{d_j^*}$	$\left(\frac{p_j^*}{p_b}\right)^{0.5}$
200	0.064	0.72	1.03
245	0.081	0.91	1.14
304	0.099	1.11	1.27
390	0.114	1.28	1.44
565	0.157	1.76	1.73
693	0.172	1.93	1.92

$y_o/d_j^* = (p_j^*/p_b)^{\frac{1}{2}}$, since $M_j = 1$]. At the highest pressure tested, the values of y_o/d_j^* for the two injectors are essentially the same, but for all lower p_{t_j}, y_o/d_j^* for the multiport injector is smaller. Of course, if a comparison is made on d_{je} instead of d_j^*, the multiport injector is considerably poorer at all pressures.

Table 2 presents the measured Mach disk heights for the five ports of the multiport injector in the aligned orientation at the single testing condition $p_{t_j} = 565$ psia.

Table 2

Mach Disk Heights for Five-Port Injector in Aligned Orientation; $p_{t_j} = 565$ psia

Injector Number	Distance to Mach Disk, y_o (in.)	y_o/d_j^*	Effective Local Pressure (psia)
1	0.14	1.61	115.0
2	0.21	2.36	53.6
3	0.28	3.15	30.1
4	0.40	4.49	14.8
5	0.57	6.40	7.3

The value of $y_o/d_j^* = 1.61$ for first Mach disk is in general agreement with the value of 1.73 from the single-hole correlation at $p_{t_j} = 565$ psia (Table 1). For ports 2-5, y_o increases monotonically, and the approximate character of the local external pressure can be obtained by using Eq. (1) with the local y_o/d_j^* and calculating p_b, the effective back pressure. These values shown in the last column of Table 2 indicate that the local p_b drops from near the single-port value corresponding to the free stream p_{t_a} (p_t' = 150 psia, and p_b = 100 psia, for $p_{t_a} = 565$ psia) to about half the free stream static pressure of 14.7 psia. Regions of static pressure of $\sim$ 0.5 p_a are known to be present in the wake of single-port injectors (e.g., see Figs. 10 and 11, Ref. 11). The displacement of the Mach disk from the fifth port (y_o = 0.57 in.) is 65% greater than that for a single port at the same p_{t_j}[$y_o = 1.73(0.2) = 0.346$ in.]. This result suggests that the aligned multiport-injector could be used effectively to enhance penetration.

Data Analysis

The experimental data presented in the preceding section have been used to deduce other fluid properties and flow parameters at axial positions at $x/d_{je} = 5$ and 10. (For the single port, $d_j^* = d_{je} = 0.200$ in.) Details of the procedure for obtaining static temperature and pressure, sound speed, the gas constant and the hydrogen mass fraction are given in the Appendix. The method by which these properties are used to deduce flow parameters, viz., the mass flux of each species and the local mass-averaged total pressure, is also discussed.

Single Port - Typical profiles of T and p/p_{t_a} for the various y/d_j^* settings and $p_{t_j}/p_b = 5.7$ are shown in Figs. 10 and 11 for $x/d_j^* =$ 5 and 10, respectively. These curves are drawn through the points calculated from the discrete data points shown in Figs. 4 and 5. From these plots the y, z coordinates of isotherms and isobars can be obtained and plotted as in Figs. 12 and 13. The nominal values of these properties in the undisturbed flow ahead of the jet are T = 214°R (for $T_{t_a} = 530$°R) and $p/p_{t_a} = 0.0417$ (for $M_a = 2.72$). From Fig. 3 the zero concentration contour is approximately circular with a radius of $\sim 3\ d_j^*$, and it is centered at $z/d_j^* = 0$, $y/d_j^* \approx 2.7$. From schlieren photographs the interaction shock passes through $y/d_j^* \approx 8$ at $z/d_j = 0$ and $x/d_j^* = 5$ and thus lies $\sim 2\ d_j^*$ outside the 0% H_2 contour at this point. If it is assumed that the same relative separation exists at other z/d_j^*, then it appears that whereas some of the flowfield surveyed lies outside the 0% H_2 contour, none of it lies outside the shock contour. Flow within this region has passed through the standoff shock and has incurred a total pressure loss which varies inversely with the distance from the injector. Downstream of the shock the flow reaccelerates and pressure, temperature, and Mach number tend to readjust to near the undisturbed free-stream values. However, regions of locally higher or lower pressure and temperature do exist because the process of flow realignment requires both expansion and compression waves to meet the requirements for compatibility of pressure and flow direction. Figure 14 shows the Mach number profiles deduced from the ratio of cone

static to pitot pressure. Contours in the immediate region of the plate where the Mach number decreases to 0 in the boundary layer have been omitted for clarity. Note that Mach numbers below 1.13, the shock detachment condition for the conical probe, are not present outside this region. The local velocity (u) and hydrogen mass flux (ρu) contours shown in Figs. 15 and 16 were obtained from the p/p_{t_a}, T, M and gas composition contours using a mass-averaged gas constant and total temperature by the method described in the Appendix. The peak velocity of 4900 ft/sec at $x/d_j = 5$, $y/d_j = 2.6$, $z/d_j = 0$ occurs in the center of the hydrogen jet downstream of the Mach disk.

Integration over the area enclosed within the mass flux distribution up to zero ρu contour in Fig. 16, assuming the arithmetic mean value of ρu for the area bounded between each pair of adjacent contour lines, led to mass flow rates of 0.099 lbm/sec at $x/d_j^* = 10$. The metered incoming flow rate based on averaged values of hydrogen plenum pressure and temperature of 550 psia and 500°R respectively, and an assumed discharge coefficient, C_D, of 0.95 is 0.103 lbm/sec. These differences of 4% (low) at $x/d_j^* = 5$ and 9% (low) at $x/d_j^* = 10$ are felt to be well within the reasonable error bounds considering the complexity of the experimental procedure and data analysis techniques.

The total pressure contours shown in Fig. 17 were deduced from the pitot pressure and Mach number plots (Figs. 4, 5 and 14) using the Mach number relationships (Ref. 15). Figure 18 shows the mass flux profiles for the mixture $(\rho u)_{mix}$ obtained in a manner similar to that used in obtaining the hydrogen mass flux contours (see Appendix). With $(\rho u)_{mix}$ and p_t defined it is now possible to obtain the mass-averaged total pressure, which is defined as

$$\overline{p}_t \equiv \left(\sum_i^N (\rho u)_{mix_i} \, p_{t_i} \right) \Big/ \left(\sum_i^N (\rho u)_{mix_i} \right) \qquad (2)$$

where the N values of $(\rho u)_{mix}$ and p_t are obtained by assigning local values to a larger number of small finite areas from Figs. 17 and 18. This procedure is first carried out over the region enclosed by the 0% H_2 contour and then extended symmetrically outward to a similarily shaped contour containing sufficient air to represent an overall stoichiometric fuel-air ratio. At large distances from the injector beyond where data were obtained, the free-stream values of $(\rho u)_{mix} = 367$ lb/sec-ft^2 and $p_t = 356$ psia were used. For the single-port injector at $x/d_j^* = 5$, $\overline{p}_t$ was 245 psia for the gas within the 0% H_2 contour and was 320 psia for the region between the 0% H_2 contour and the contour enclosing sufficient air for stoichiometric proportions. At $x/d_j^* = 10$ the corresponding values were 209 psia and 340 psia. The losses in total pressure from the original values of 356 psia for the air and 550 psia for the hydrogen include the interaction losses, the losses due to mixing and the wall shear. Since the mixing losses are dependent on the degree of mixing it is necessary to consider the extent of mixing in

comparing total pressure losses. A reasonable basis for comparison would be the mass-averaged total pressure at the point where the stream reached uniform stoichiometric proportion. The latter condition could only be attained, of course, inside a combustor duct with the correct overall fuel-air ratio, whereas in the unbounded case treated experimentally here, a gradient in ER would always exist. Moreover, to calculate the total pressure loss a rigorous coaxial, but not axisymmetric, mixing analysis would be required. To avoid this difficulty and yet still obtain a comparison of the total pressure loss which accounts for the difference in degree of mixing, the following approximate analysis was made. For each of the two streams (i.e., stream 1 is within the 0% H_2 contour and stream 2 is between the 0% H_2 contour and the stoichiometric air contour) the mass-averaged total pressure and ρu_{mix} and average H_2 concentration (zero for the outside stream) are known. Thus, mass-averaged properties can be assigned to each stream. If it is then assumed that the two streams mix uniformly in a constant-area process in the absence of wall shear, then the conservation equations can be solved for the mass-averaged properties of the uniformly mixed stream. For example, given the case herein of $T_{t_j} \approx T_{t_a}$, $\gamma_j = \gamma_a = 1.4$, the expression for the mass-averaged Mach number M_3 is obtained from the implicit equation

$$\frac{1 + \gamma M_3^2}{\Gamma_3} = \frac{\frac{P_1 A_1}{P_2 A_2}(1 + \gamma M_1^2) + (1 + \gamma M_2^2)}{\frac{P_1 A_1}{P_2 A_2}\Gamma_1 + \Gamma_2} \tag{3}$$

where

$$\Gamma(M) = (R)^{-\frac{1}{2}} M \left[1 + \frac{\gamma - 1}{2} M^2\right]^{\frac{1}{2}} \tag{4}$$

With M_3, and $A_3 = A_1 + A_2$, the other properties are readily obtained. The "mixed" average total pressures obtained by this method were 254 psia from the $x/d_j^* = 5$ data and 242 psia from the $x/d_j^* = 10$. Part of the 12 psia (or 5%) difference would be due to the wall shear between $x/d_j^* = 5$ and 10 and part is probably due to inherent inaccuracy in the calculational procedure. Table 3 shows mass-averaged properties for $x/d_j^* = x/d_{je} = 5$.

Multiple Port - Isotherms and isobars deduced from the cone-static and pitot pressure data presented in Figs. 7 and 8 are shown in Figs. 19 and 20 for both perpendicular and aligned injectors at $x/d_{je} = 5$. Mach numbers deduced from the pressures are shown in Fig. 21. With the injector in the perpendicular configuration, crests and troughs in the Mach number profiles are evident for regions near the plate. For a fixed y/d_{je} the Mach numbers are slightly higher for regions close to the center port at $z/d_{je} \simeq 0$ than for the outermost ports. Note that the individual Mach contours are not symmetrical about the fuel injector ports. Apparently, a considerable amount of interaction occurs between the hydrogen jets during expansion for small values of the ratio of port center-to-center

spacing to port diameter (ℓ/d_j* = 3). With the five-hole injector aligned with the flow, the Mach number contours are more regular.

The local velocity (u), hydrogen mass flux $(\rho u)_{H_2}$ and air-hydrogen mass flux $(\rho u)_{mix}$ contours in Figs. 22, 23, and 24 were obtained from the static values of p and T (see Appendix), the M-contour data, a mass-averaged gas constant, and the hydrogen concentration data assuming a two-component mixture of ideal gases.

An area integration of the hydrogen mass flux distribution, assuming the arithmetic mean value of $(\rho u)_{H_2}$ for the entire area bounded between each pair of adjacent contour lines, led to mass flow rates of 0.090 lbm/sec for the aligned orientation (Fig. 23a) and to 0.088 lbm/sec for the perpendicular orientation (Fig. 23b). The metered incoming flow rate based on an averaged plenum hydrogen pressure and temperature of 565 psia and 535°R, respectively, and a calibrated discharge coefficient, C_D, of 0.96 is 0.10 lbm/sec. The integrated mass flows are 10% low and 12% low for the aligned and perpendicular configurations, respectively. These results are comparable to the 4%-low agreement obtained for the single 0.200-inch port, considering the increased complexity of the near downstream flow field resulting from multiple-port injection.

The total-pressure profiles in Fig. 25 were obtained from pitot pressure and deduced Mach number data. Mass-averaging of the total pressure was performed by first constructing a grid of local $(\rho u)_{mix}$ and p_t values obtained by superimposing the $(\rho u)_{mix}$ contours of Fig. 24 on the p_t contours of Fig. 25 and then carrying out the averaging procedure of Eq. (2). For the perpendicular orientation, the p_t within the zero H_2 concentration contour was 205 psia, while for the aligned orientation it was 233 psia. The values for mass-averaged total pressure for the region between the 0% H_2 boundary and the boundary for ER = 1 are 309 psia for the perpendicular orientation and 344 psia for the aligned orientation. Mass-averaged properties for the gas within the 0% H_2 contour (stream 1), the air added to bring the mixture to stoichiometric (stream 2), and the "mixed" condition (stream 3), as defined above, are listed in Table 3.

Table 3

Mass-Averaged Properties Based on Data at x/d_{je} = 5

Injector Configuration	Stream 1				Stream 2 (ER = 0)			Mixed to ER = 1		
	ER	p, psia	M	p_t, psia	p, psia	M	p_t, psia	p, psia	M	p_t, psia
Single Port	2.25	10.9	2.68	245	17.9	2.53	320	13.8	2.55	254
5-Hole, Aligned	1.76	12.2	2.57	233	20.2	2.50	344	14.8	2.50	253
5-Hole, Perpendicular	2.80	10.6	2.58	205	17.3	2.54	309	15.0	2.40	220

The total pressure losses include those associated with the stand-off shock in the main stream, the barrel shock structure in the secondary jet, and losses due to mixing and wall shear. Whereas the momentum of the secondary jet is lost with cross-stream injection, the net effect on total pressure recovery due to the stream interaction can be beneficial. This arises from the fact that the compression in the main stream lowers the Mach number at which mixing takes place, and the mixing losses are lower. Coaxial injection can also cause a compression in the main stream but in general, the attendant pressure rise would be less than with cross-stream injection.

To demonstrate this effect and at the same time provide a comparative basis for the experiments discussed herein, consider the following exemplary cases. Coaxial constant-area mixing of an air stream at $M = 2.72$ with a hydrogen jet at $M = 1$ with the experimental values for the initial total pressures, i.e., $p_{t_a} = 356$ psia, $p_{t_j} = 565$ psia, and $T_{t_a} = T_{t_j} = 530°R$, in stoichiometric proportions, results in a mixed total pressure of 186 psia. On the other hand, if the hydrogen jet had been initially expanded to the air stream static pressure of 14.83 psia, $M_j = 3.024$ prior to mixing, then the mixed total pressure would be 195 psia. With cross-stream injection and no compression in the mainstream the corresponding mixed total pressures would be 133 psia for either $M_j = 1$ or $M_j = 3.024$, since the initial momentum of the fuel is lost. If, however, the secondary injection causes a compression in the mainstream, pressure recoveries can be appreciably higher. For example, if the interaction causes a compression equivalent to an oblique turning angle of 18.9° with a corresponding pressure ratio of 3.25, then the mixed total pressure for $M_j = 1$ and coaxial injection becomes 236 psia. With cross-stream injection and the model constrained to that of the mixed jet area set equal to area of the primary streamtube following compression, the comparison can not be made. This is because the Mach number in the mixed stream is 1.06 without compression and even the slightest compression would produce sonic mixed conditions. However, if the model is constrained to constant pressure instead of constant area, then a comparison can be made. For a constant-pressure process with cross-stream injection and no compression, the mixed total pressure is 93 psia, but with compression equivalent to 18.9° of turning, the mixed total pressure is 152 psia. Oblique compressions of other strengths would of course produce either higher or lower values of mixed total pressure.

These example cases show that constant-area mixing processes yield higher mixed total pressures than constant-pressure processes, much the same as in heat-addition processes. Precompression prior to mixing results in appreciably lower total-pressure losses. Comparison of the experimental results with those of the simple two-stream model indicates that the precompression due to the strong shock in the mainstream is the probable cause for the relatively high deduced total pressures.

CONCLUDING REMARKS

This detailed study of the near-field distributions of properties resulting from the transverse (normal) injection of hydrogen from flush wall ports into a Mach 2.72 air stream has shown that:

1) A small improvement ($\sim$ 7%) in area coverage of fuel distribution in the transverse plane at $x/d_{je} = 5$ for a given fuel mass flow can be obtained by replacing one larger fuel port by a row of five smaller ports aligned in the flow direction. (Here x is the distance downstream from the center of the injector and d_{je} is the diameter of the one larger port.) If the same row of five smaller ports is oriented in the cross-stream direction, however, the area coverage decreases by $\sim$ 12%, and the total-pressure loss for the main stream increases. The reduction in area coverage results from a large decrease ($\sim$ 40%) in vertical penetration distance from the plate that is only partially compensated by better lateral coverage. Thus, interaction between adjacent jets in the lateral direction is unfavorable to fuel distribution for the fuel port spacing used in this study (3-diameter center-to-center spacing). Because some finite lateral spacing will be needed in any practical engine system, further studies are needed to define the minimum spacing at which this unfavorable interaction becomes negligible.

2) From a combination of cone-static-pressure, pitot-pressure, and hydrogen-concentration measurements and many data analysis steps it was possible to deduce hydrogen mass flux distributions with sufficient accuracy that their integrals in the plane at $x/d_{je} = 5$ agreed with the metered hydrogen input mass flows to within 4% to 12% (always low). Such agreement is considered to be quite good in view of the number of data manipulations involved and the complexity of the flow field, and it confirms the usefulness of the data reduction procedures for $x/d_{je} \geq 5$.

3) From the deduced profiles at $x/d_{je} = 5$ and a simple constant-area mixing approximation it was possible to estimate equivalent air total pressure recoveries for the production of uniform, stoichiometric mixtures. These recoveries were 71% for the single-port injector and the aligned multiport injector, and 61% for the cross-flow orientation of the multiport injector. The fact that the loss for the multiport injector in the cross-flow orientation is appreciably higher than that for a single port further enforces the need for studying the spacing effect as noted under (1). Even though the losses in total pressure are substantial, they are appreciably smaller than would occur without precompression in the primary stream with either coaxial or transverse injection. It appears from these results that the proper consideration of the shock interaction is one of the more important factors in the evaluation of a particular method of injection.

APPENDIX

All of the derived properties of the flow are based on the ideal gas relationships for $\gamma = 1.4$, since all gases present are diamotic at the conditions tested. On the other hand in the derivation of properties dependent on the gas constant the local mass fraction of each component has to be considered; i.e., the gas constant for the mixture, R_{mix}, is given by

$$R_{mix} = R^{o} \sum_{i}^{N} Y_i / \mathfrak{m}_i \tag{A-1}$$

where

Y_i mass fraction of the i^{th} component

$\mathfrak{m}_i$ molecular weight of the i^{th} component

R^{o} universal gas constant, 1545.32 ft-lb_f/lb_m-°R

For the hydrogen-air mixture

$$R_{mix} = R^{o} \left(\frac{Y_{H_2}}{2.016} + \frac{Y_{air}}{28.995} \right) \tag{A-2}$$

where

$$Y_{air} = 1 - Y_{H_2}$$

and hydrogen mass fraction Y_{H_2} is given by

$$Y_{H_2} = \frac{X_{H_2} \mathfrak{m}_{H_2}}{\left(1-X_{H_2}\right) \mathfrak{m}_{air} + X_{H_2} \mathfrak{m}_{H_2}} = \frac{X_{H_2}}{\left(1-X_{H_2}\right) \frac{28.995}{2.016} - X_{H_2}} \tag{A-3}$$

where the hydrogen mole fraction X_{H_2} is obtained from the gas-chromatographic analysis of the samples. It is assumed that the local total temperature is the sum of the hydrogen and air plenum temperatures weighted by their respective mass fractions:

$$T_{t_{mix}} = T_{t_{H_2}} Y_{H_2} + T_{t_{air}} Y_{air} \tag{A-4}$$

The local Mach number is determined from the ratio of cone surface pressure p_c to pitot pressure p_t' using either conical shock tables (Ref. 13) or, in the case of machine data reduction, a ninth-degree polynominal expression (Ref. 10) as follows:

$$M = 1.19999 + 0.58974\ Z + 0.39513\ Z^2 + 0.59601\ Z^3$$
$$- 3.19487\ Z^4 + 16.42127\ Z^5 - 44.28010\ Z^6$$
$$+ 65.16608\ Z^7 - 48.38444\ Z^8 + 14.48614\ Z^9 \qquad \text{(A-5)}$$

which is applicable over the range

$$0.1748 < p_s/p_t' < 0.5438; \quad \theta = 15 \text{ deg}$$

where

$$Z = - 2.71003\ (p_c/p_t') + 1.47371$$

With Mach number and mixed total temperature defined, the local static pressure p is obtained from the Rayleigh pitot formula (Ref. 15) and p_t and T_{mix} from the isentropic flow relationships (Ref. 15). The local (mixture) flow velocity is given by

$$u = M\ a \qquad \text{(A-6)}$$

where a, the sound speed (in ft/sec) is given by

$$a = 263 \sqrt{T_{mix}/m_{mix}} = 263 \sqrt{(R_{mix}/R^o)T_{mix}} \qquad \text{(A-7)}$$

The local mixture density (lb_m/ft^3) needed to compute the local mass flux $(\rho u)_{mix}$ (lb_m/ft^2-sec) is given by

$$\rho_{mix} = p/R_{mix}\ T_{mix} \qquad \text{(A-8)}$$

and the hydrogen mass flux, $(\rho u)_{H_2}$ is obtained from

$$(\rho u)_{H_2} = Y_{H_2}\ (\rho u)_{mix} \qquad \text{(A-9)}$$

Point values of a, Y_{H_2}, $(\rho u)_{mix}$ and $(\rho u)_{H_2}$ are calculated for selected intervals in z/d_j^* (generally from 0.15 to 0.50) for each value of $y/d_j^* \geq 0.625$ (the closest distance to the plate that was surveyed) up to positions in z/d_j^* and y/d_j^* where the hydrogen concentration is zero. These profiles are then crossplotted to aid in the determination of the maps presented.

REFERENCES

1. Schetz, Joseph A.; and Billig, Frederick S.: Penetration of Gaseous Jets Injected into a Supersonic Stream. J. Spacecraft and Rockets, vol. 3, no. 11, Nov. 1966, pp. 1658-1665.

2. Orth, Richard C.; and Funk, John A.: An Experimental and Comparative Study of Jet Penetration in Supersonic Flow. J. Spacecraft and Rockets, vol. 4, no. 9, Sept. 1967, pp. 1236-1242.

3. Schetz, Joseph A.: Interaction Shock Shape for Transverse Injection in Supersonic Flow. J. Spacecraft and Rockets, vol. 7, no. 2, Feb. 1970, pp. 143-149.

4. Orth, R. C.; Schetz, J. A.; and Billig, F. S.: The Interaction and Penetration of Gaseous Jets in Supersonic Flow. NASA CR-1386, 1969.

5. Billig, Frederick S.; Orth, Richard C.; and Lasky, Marshall: A Unified Approach to the Problem of Gaseous Jet Penetration into a Supersonic Stream. AIAA Pap. No. 70-93, Jan. 1970.

6. Torrence, Marvin G.: Concentration Measurements of an Injected Gas in a Supersonic Stream. NASA TN D-3860, 1967.

7. Chrans, Larry J.; and Collins, Daniel J.: Stagnation Temperature and Molecular Weight Effects in Jet Interaction. AIAA Journal, vol. 8, no. 2, Feb. 1970, pp. 287-293.

8. Povinelli, Frederick P.; Povinelli, Louis A.; and Hersch, Martin: Supersonic Jet Penetration (Up to Mach 4) into a Mach 2 Air Stream. AIAA Pap. No. 70-92, Jan. 1970.

9. Swalley, Frank E.: Measurement of Flow Angularity at Supersonic and Hypersonic Speeds with the Use of a Conical Probe. NASA TN D-959, 1961.

10. Volluz, R. J.: Handbook of Supersonic Aerodynamics, Section 20, Wind Tunnel Instrumentation and Operation. NAVORD Report 1488, vol. 6, 1961.

11. Zukoski, Edward E.; and Spaid, Frank W.: Secondary Injection of Gases into a Supersonic Flow. AIAA Journal, vol. 2, no. 10, Oct. 1964, pp. 1689-1696.

12. Kaufman, Louis G., II: Hypersonic Flow Past Transverse Jets. J. Spacecraft and Rockets, vol. 4, no. 9, Sept. 1967, pp. 1230-1235.

13. Sims, J. L.: Tables for Supersonic Flow around Right Circular Cones at Zero Angle of Attack. NASA SP-3004, 1964.

14. Chriss, E. D.: Experimental Study of the Turbulent Mixing of Subsonic Axisymmetric Gas Streams. ARO Inc., AEDC-TR 68-133, Aug. 1968.

15. Ames Research Staff: Equations, Tables and Charts for Compressible Flow. NACA Report 1135, 1953.

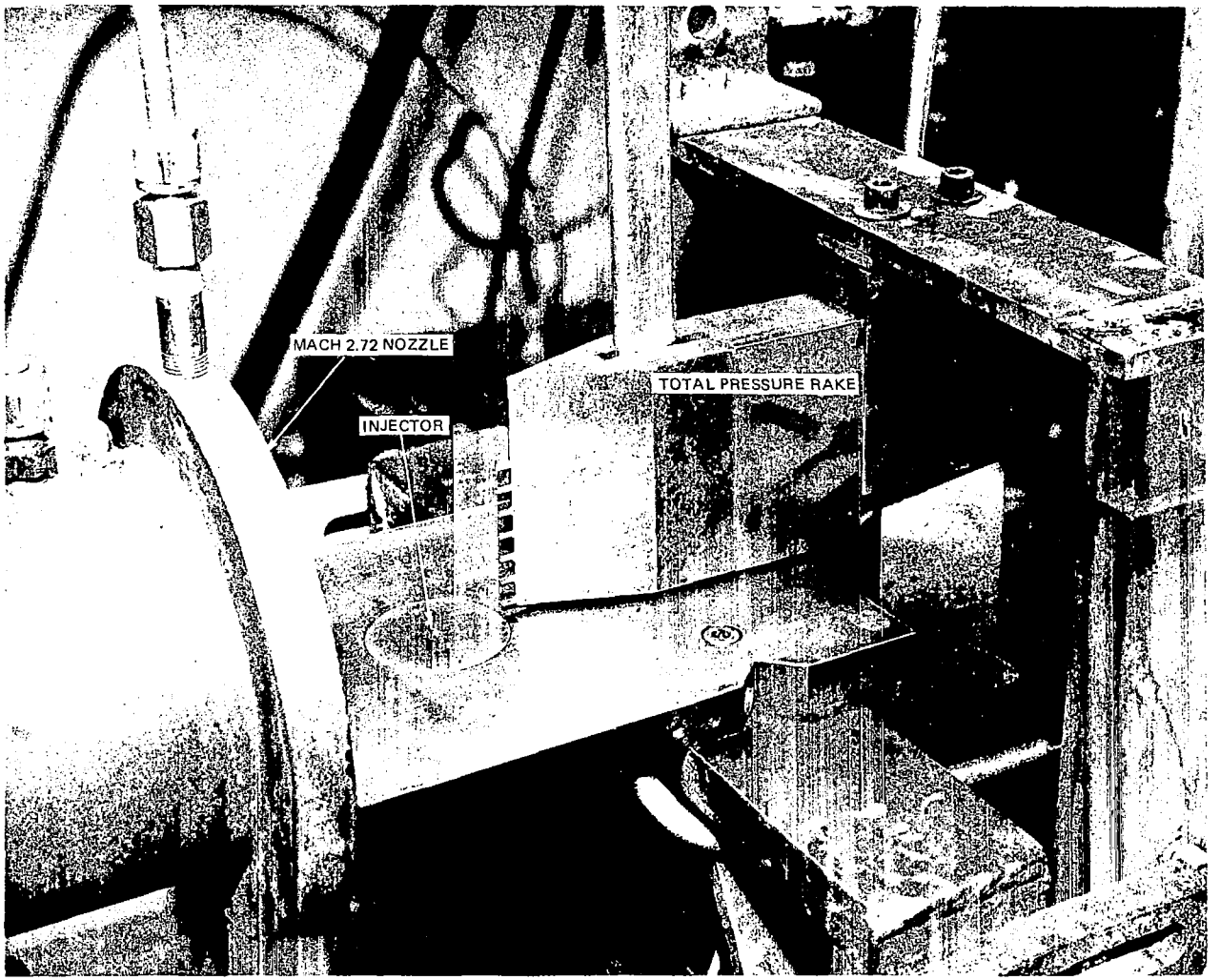

FIG. 1 FLAT PLATE INJECTOR MODEL SHOWING TOTAL PRESSURE RAKE

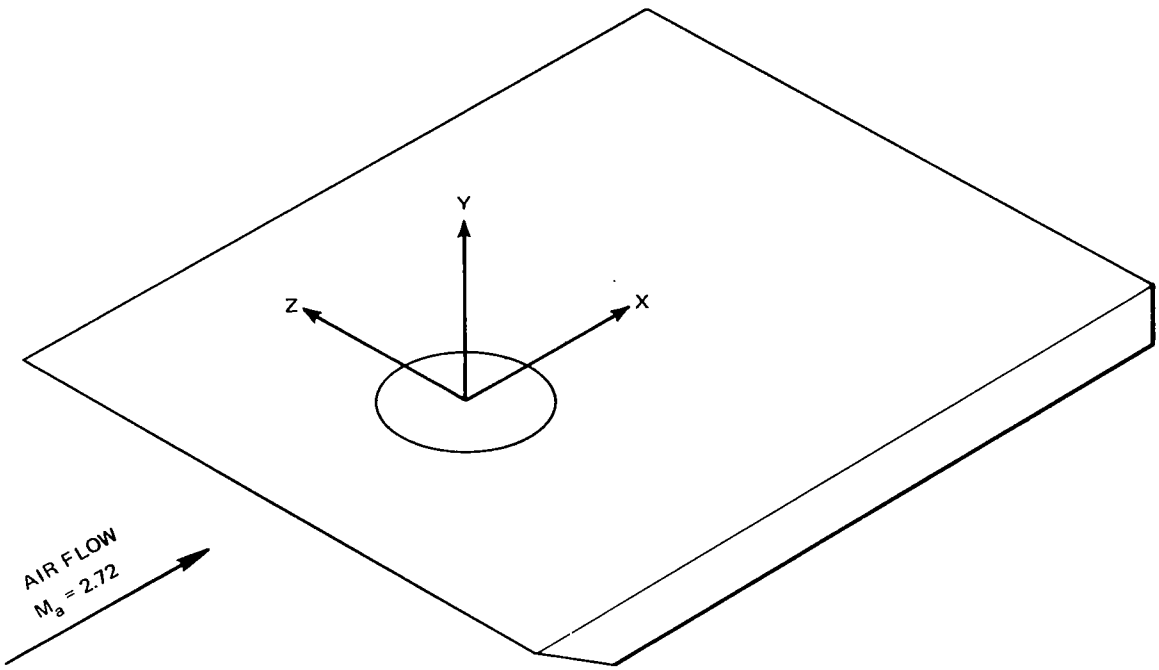

FIG. 2 SCHEMATIC SHOWING SYSTEM OF AXES

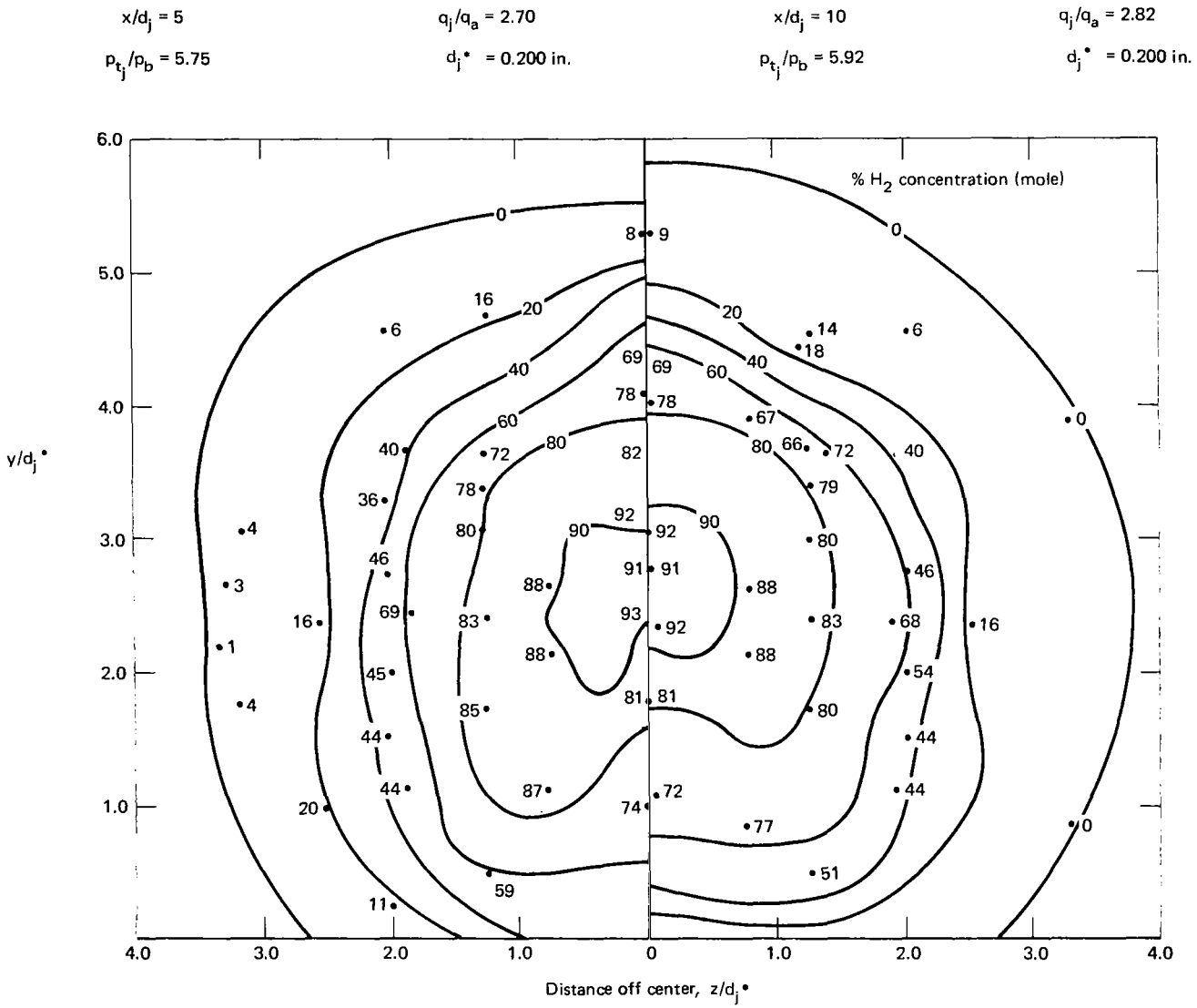

FIG. 3 CONCENTRATION PROFILES FOR SONIC INJECTION FROM A SINGLE PORT INTO A MACH 2.7 AIRSTREAM

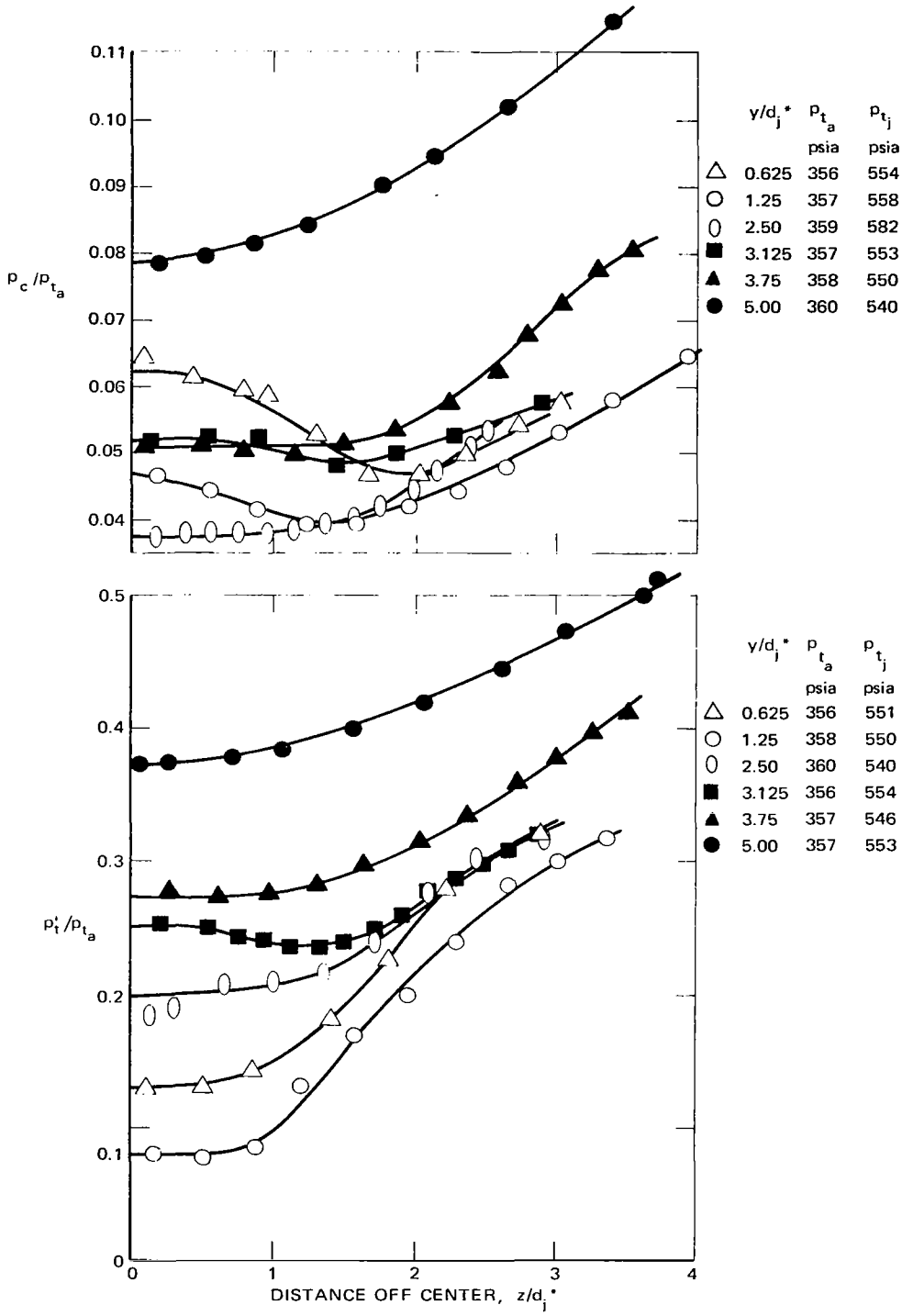

FIG. 4 MEASURED CONE SURFACE PRESSURE DATA AND PITOT PRESSURE DATA FOR A SINGLE-PORT INJECTOR AT $x/d_j^* = 5$

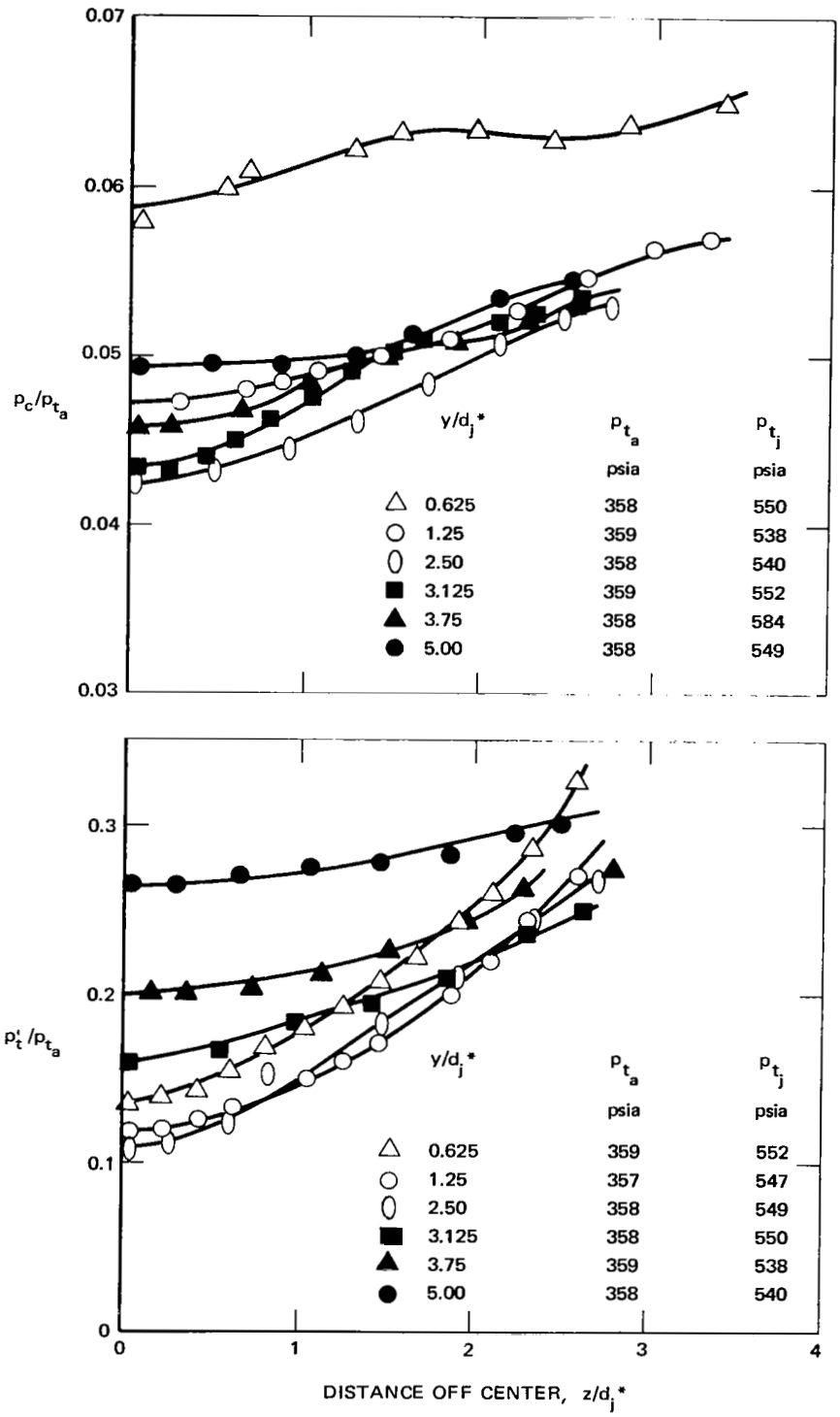

FIG. 5 MEASURED CONE SURFACE PRESSURE DATA AND PITOT PRESSURE DATA FOR A SINGLE-PORT INJECTOR AT $x/d_j^* = 10$

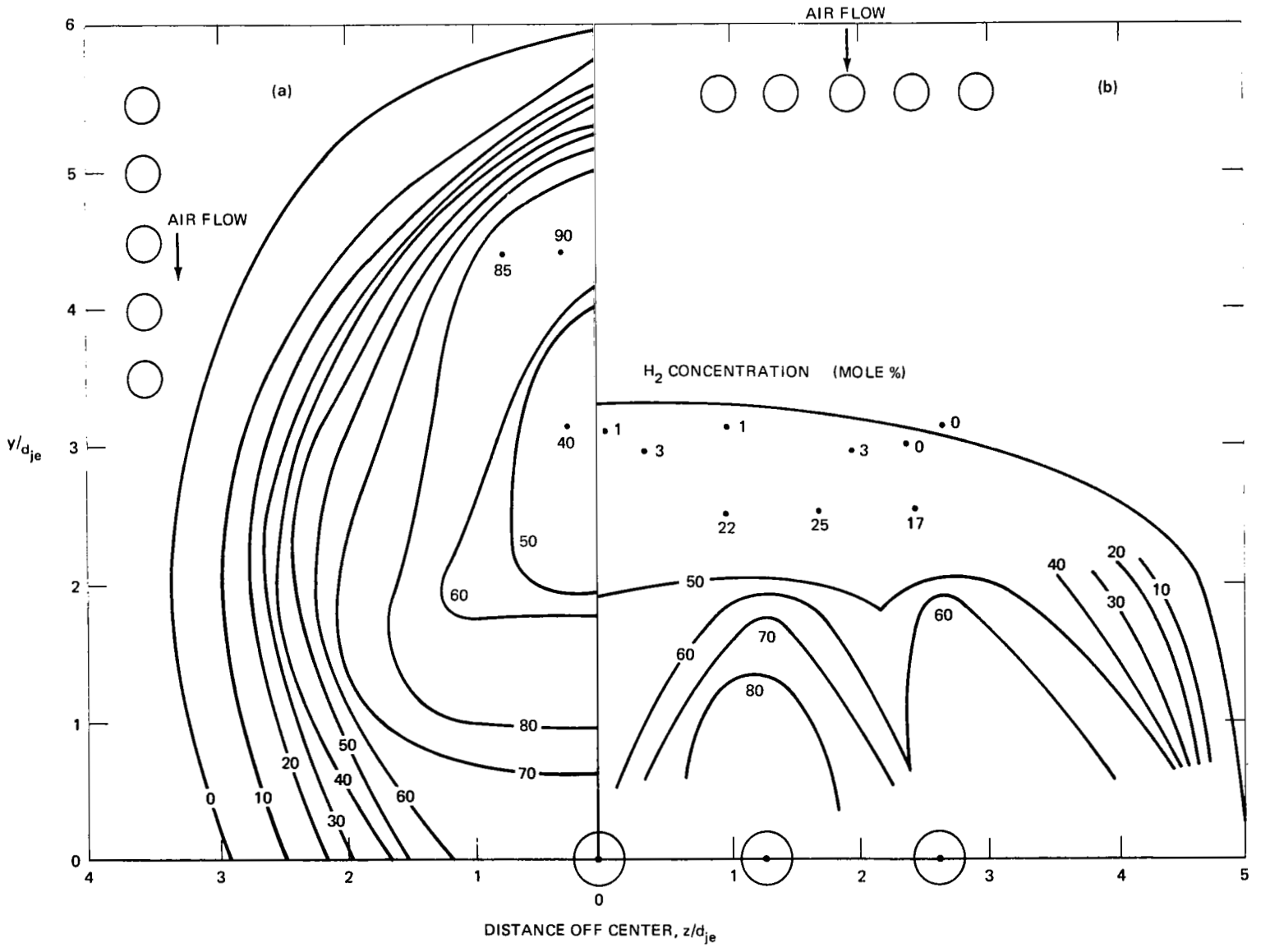

FIG. 6 CONCENTRATION PROFILES AT $x/d_{j_e} = 5.00$ FOR UNDEREXPANDED SONIC INJECTION FROM A FIVE-PORT INJECTOR INTO A MACH 2.7 STREAM FOR THE TWO ORIENTATIONS

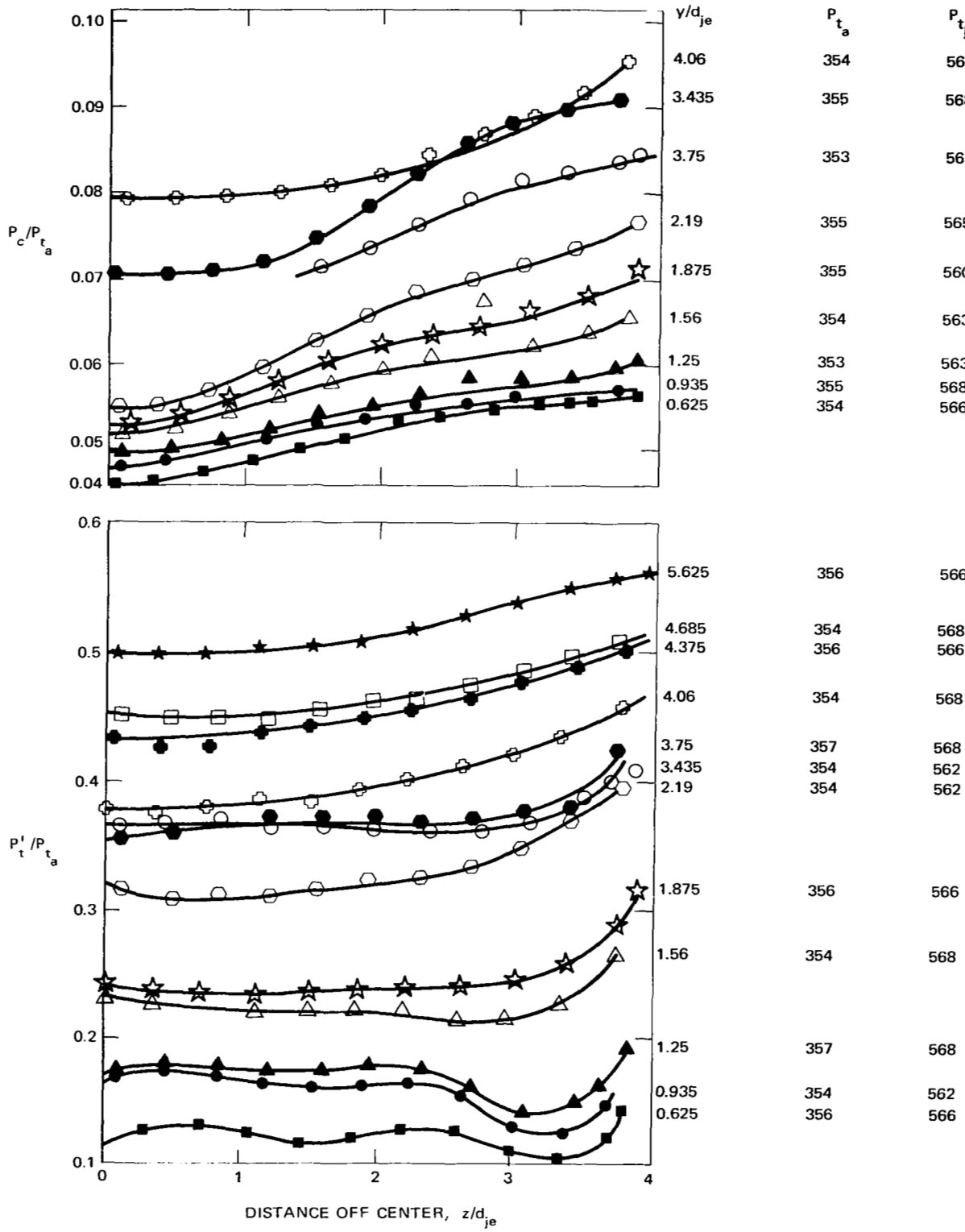

FIG. 7 MEASURED CONE SURFACE PRESSURE DATA AND PITOT PRESSURE DATA FOR FIVE-PORT INJECTOR PERPENDICULAR TO FLOW AT $X/d_{je} = 5$

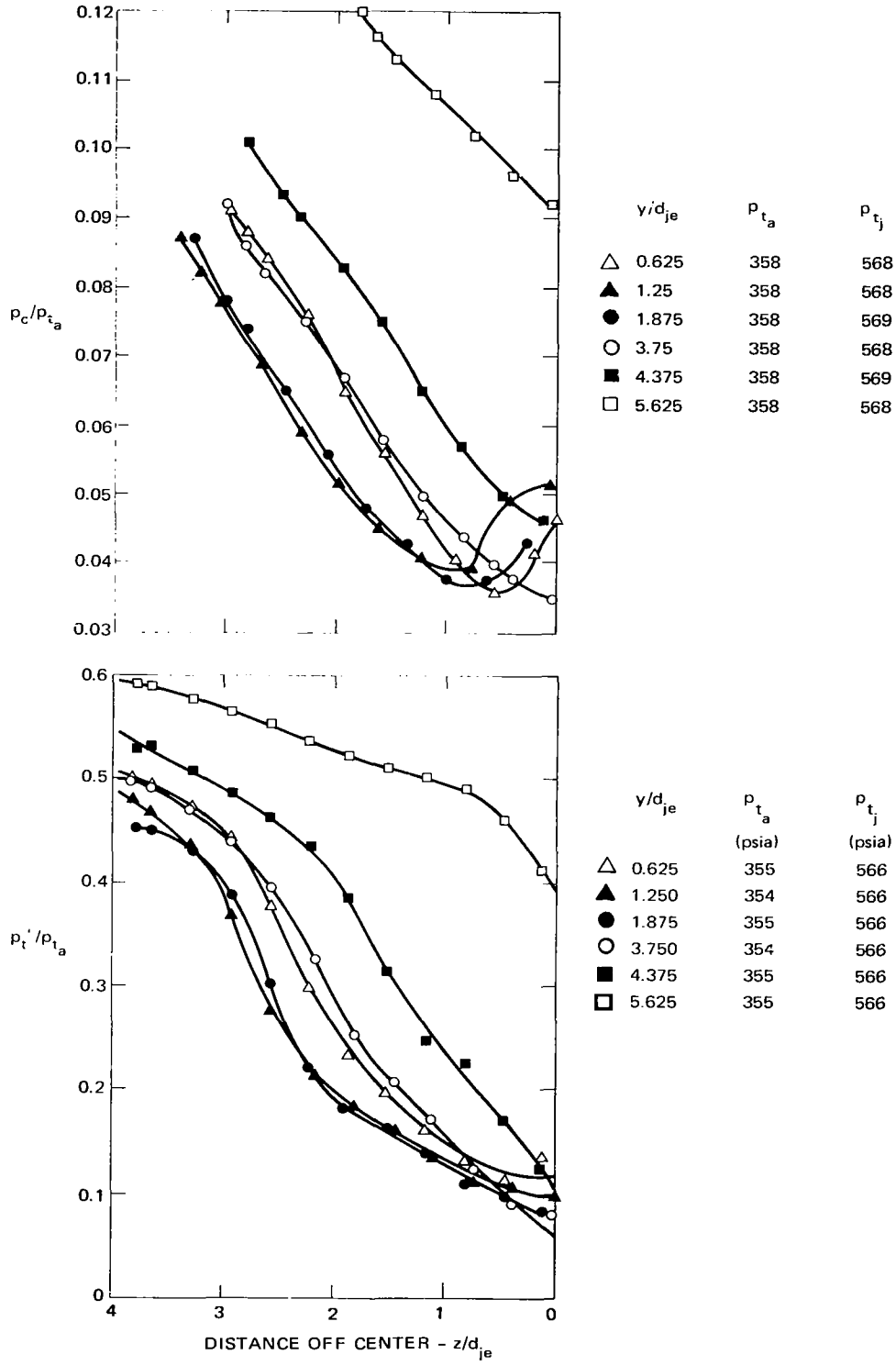

FIG. 8 MEASURED CONE SURFACE PRESSURE DATA AND PITOT PRESSURE DATA FOR FIVE–PORT INJECTOR ALIGNED WITH FLOW AT $x/d_{je}= 5$

PERPENDICULAR TO FLOW

ALIGNED WITH FLOW

FIG. 9 SCHLIEREN PHOTOGRAPHS OF JET STRUCTURE FOR SONIC INJECTION FROM A FIVE-PORT INJECTOR (P_{T_j}/P_b = 5.7) INTO A MACH 2.7 STREAM

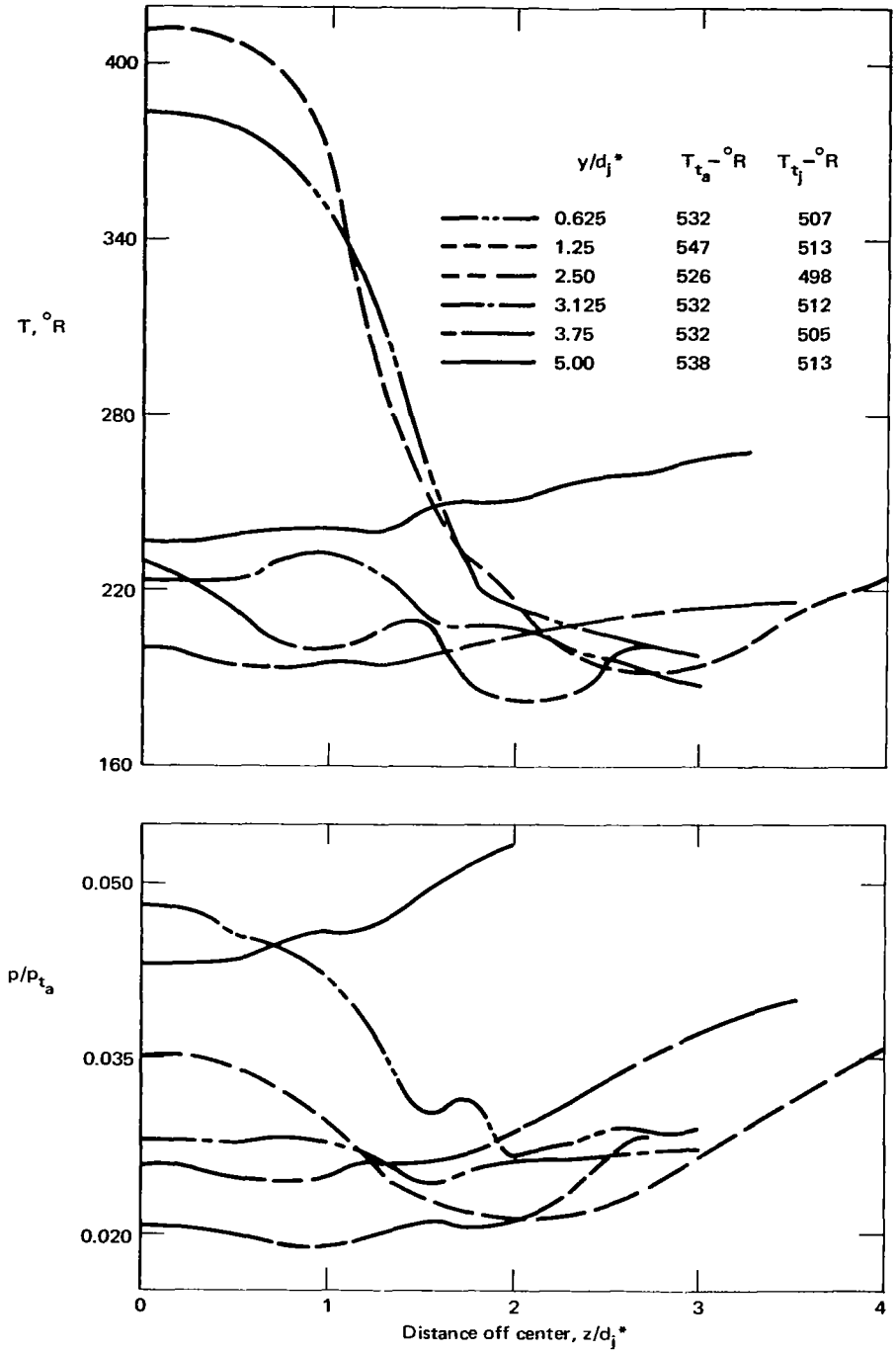

FIG. 10 DEDUCED STATIC TEMPERATURE AND PRESSURE PROFILES FOR THE SINGLE-PORT INJECTOR AT $x/d_j^* = 5$

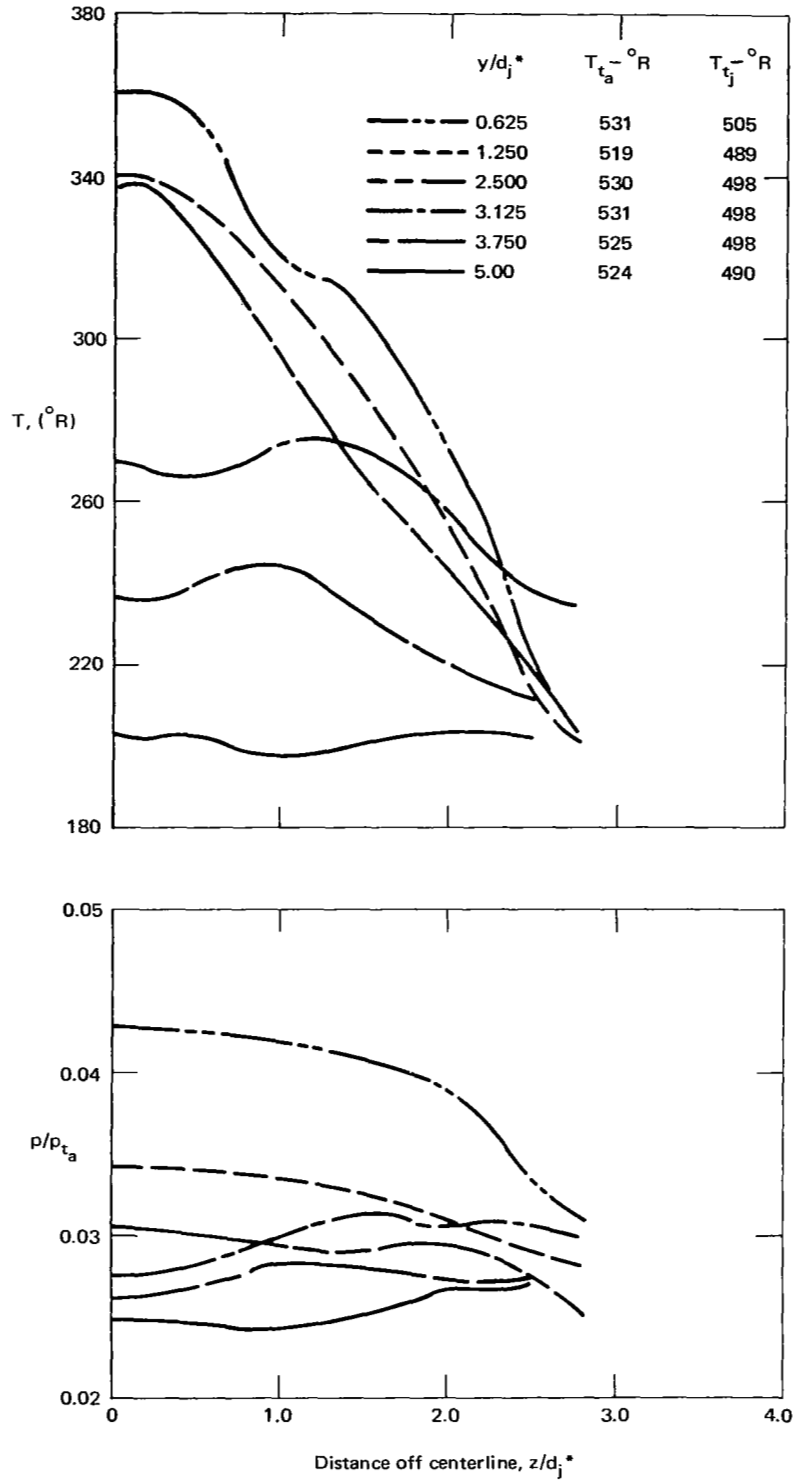

FIG. 11 DEDUCED STATIC TEMPERATURE AND PRESSURE PROFILES FOR THE SINGLE-PORT INJECTOR AT $x/d_j^* = 10$

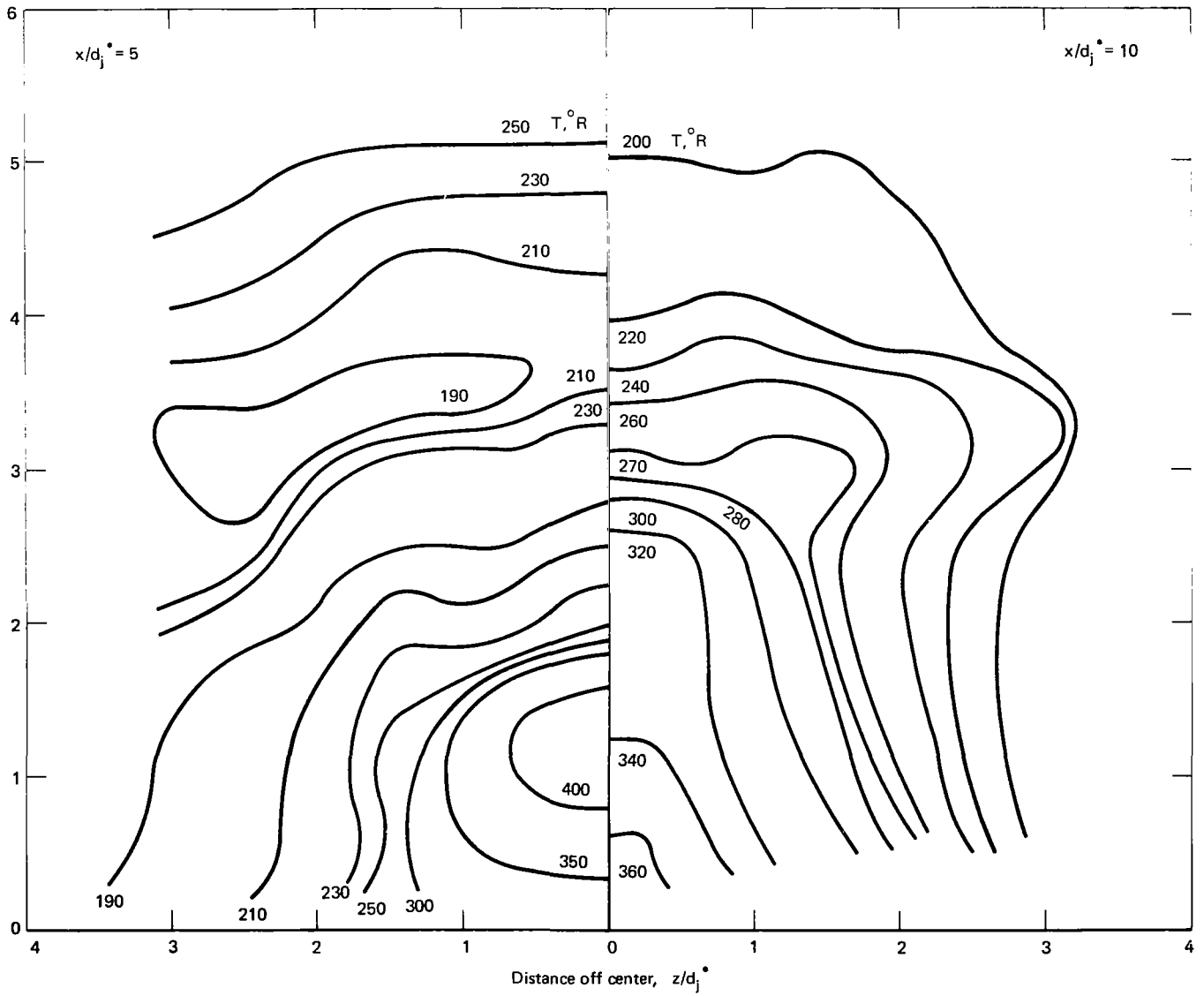

FIG. 12 DEDUCED ISOTHERMS AT TWO NONDIMENSIONAL AXIAL STATIONS, $x/d_j^* = 5$ AND 10, FOR THE SINGLE PORT INJECTOR

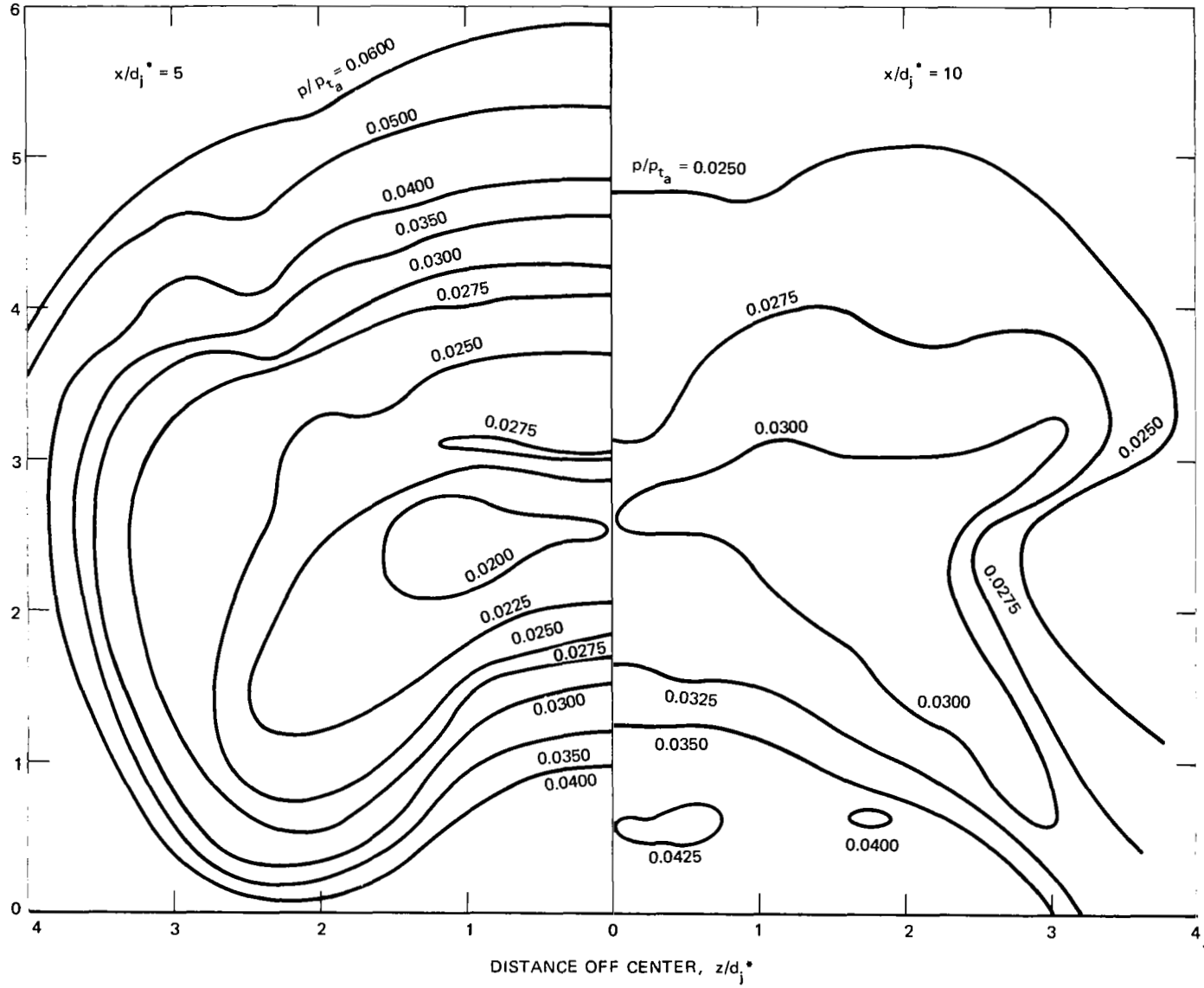

FIG. 13 DEDUCED ISOBARS AT TWO NONDIMENSIONAL AXIAL STATIONS, $x/d_j^* = 5$ AND 10 FOR THE SINGLE PORT INJECTOR

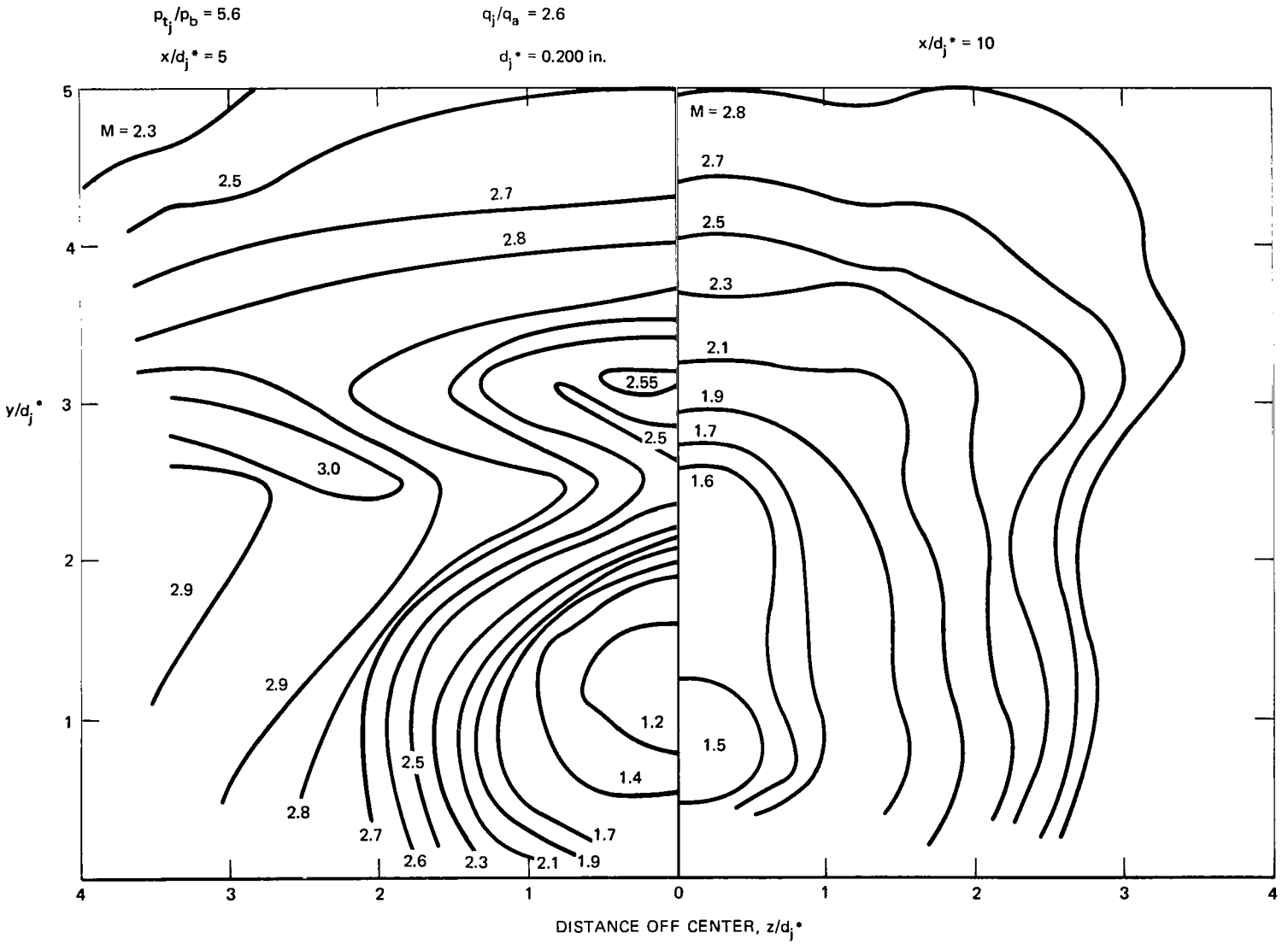

FIG. 14 DEDUCED MACH NUMBER CONTOURS AT TWO STATIONS FOR THE SINGLE PORT INJECTOR

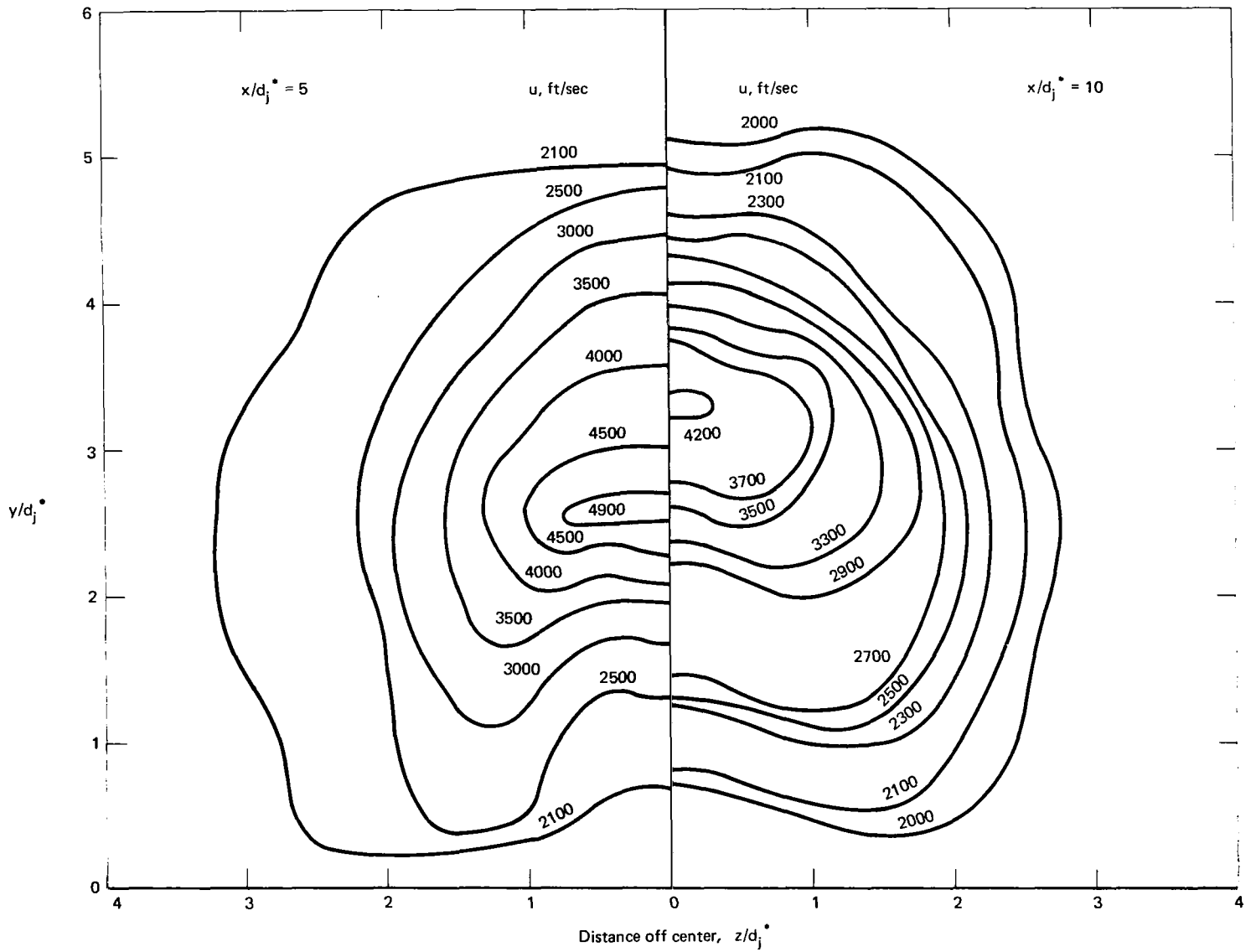

FIG. 15 DEDUCED VELOCITY CONTOURS AT TWO STATIONS FOR THE SINGLE-PORT INJECTOR

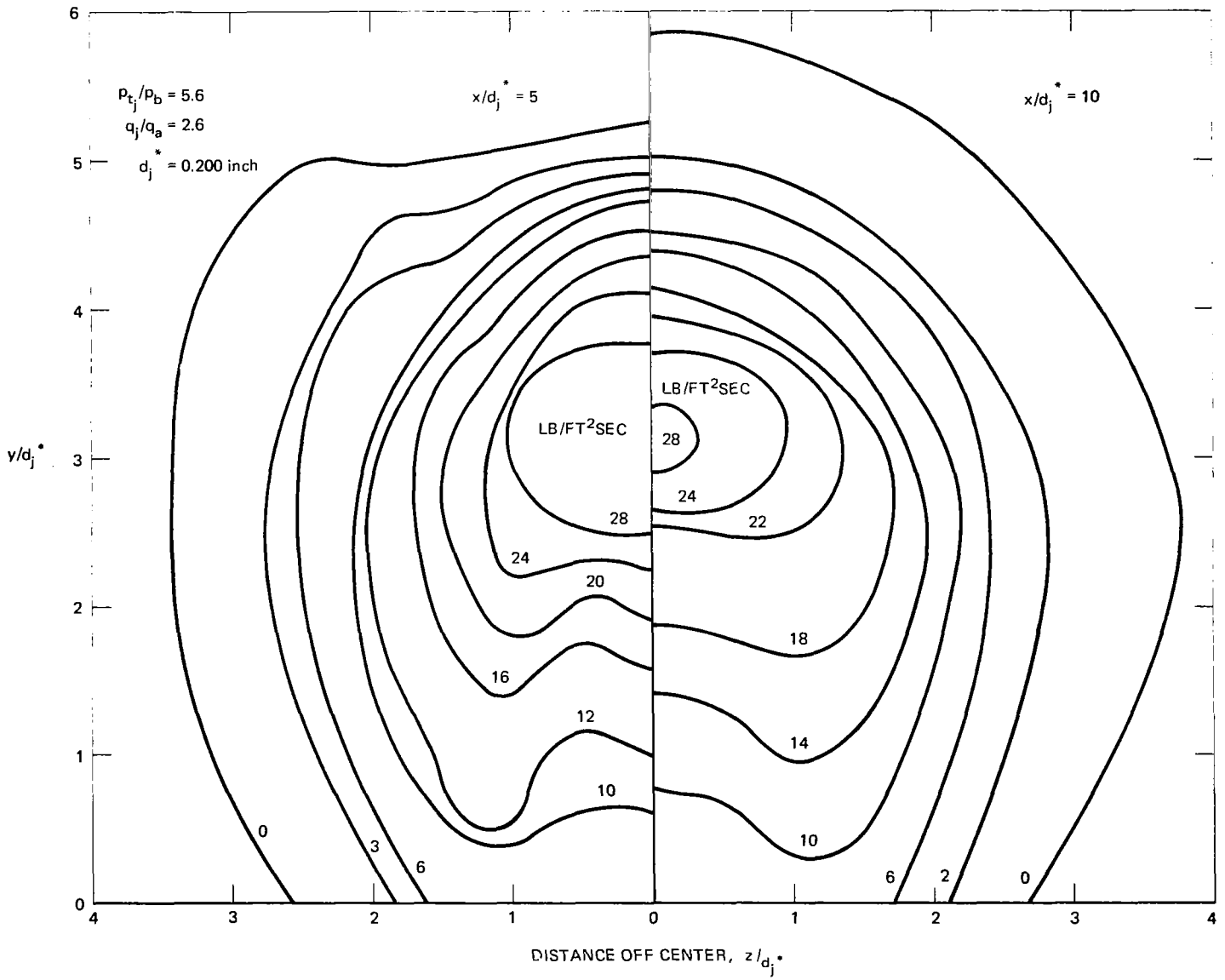

FIG. 16 DEDUCED HYDROGEN MASS FLUX AT TWO STATIONS FOR THE SINGLE-PORT INJECTOR

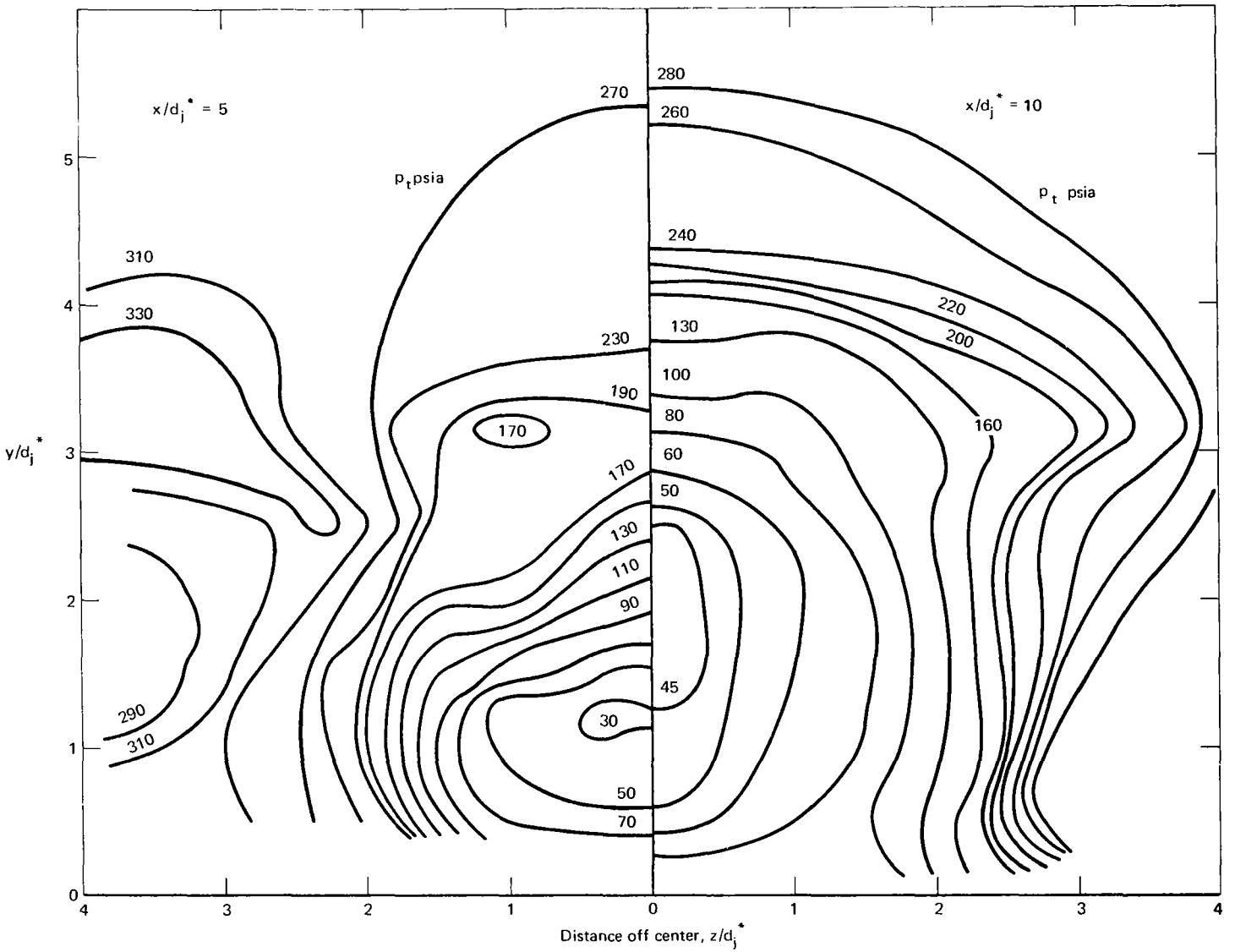

FIG. 17 DEDUCED TOTAL PRESSURE CONTOURS FOR SINGLE PORT INJECTOR

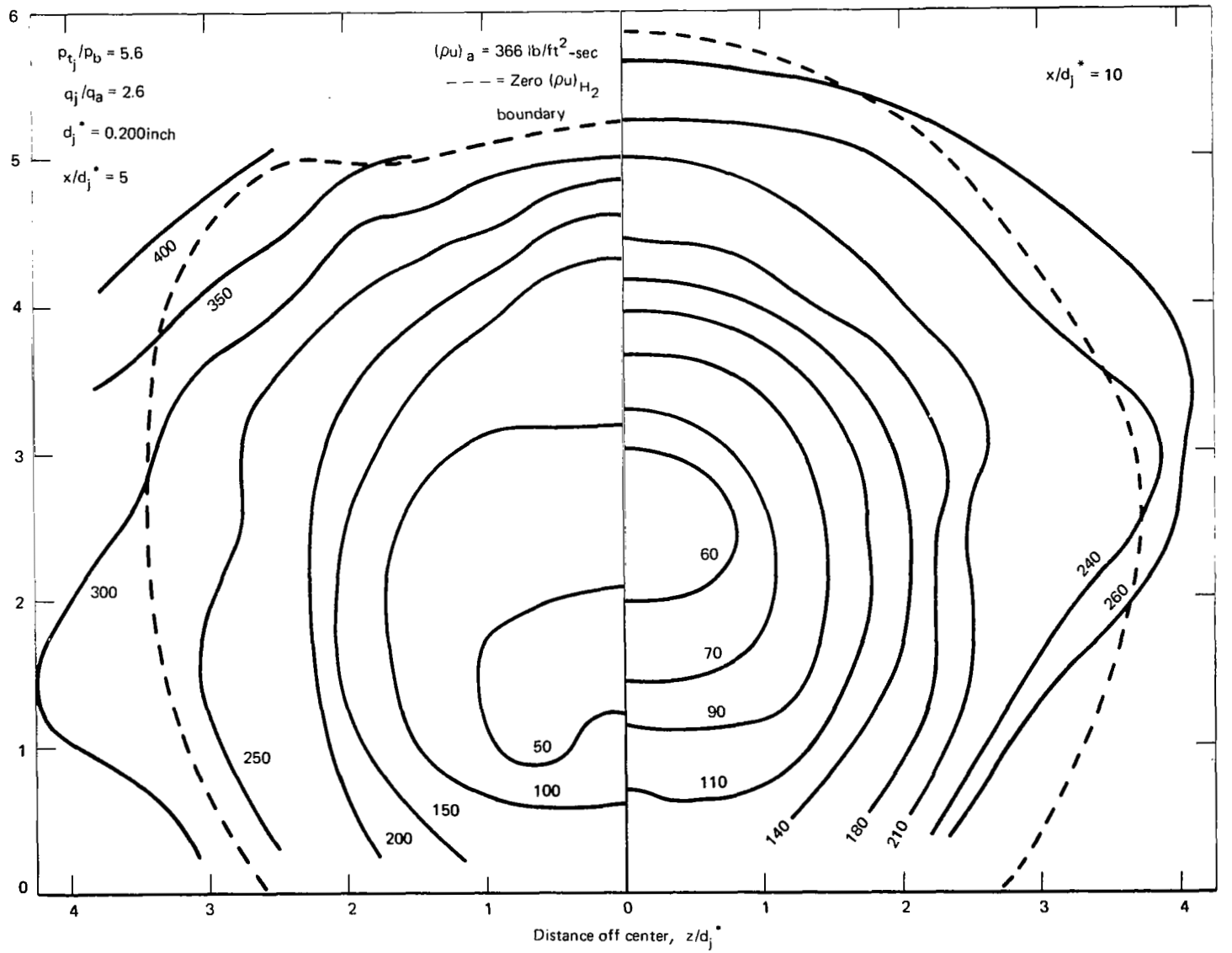

FIG. 18 DEDUCED MASS FLUX CONTOURS FOR AIR HYDROGEN MIXTURE FOR SINGLE - PORT INJECTOR

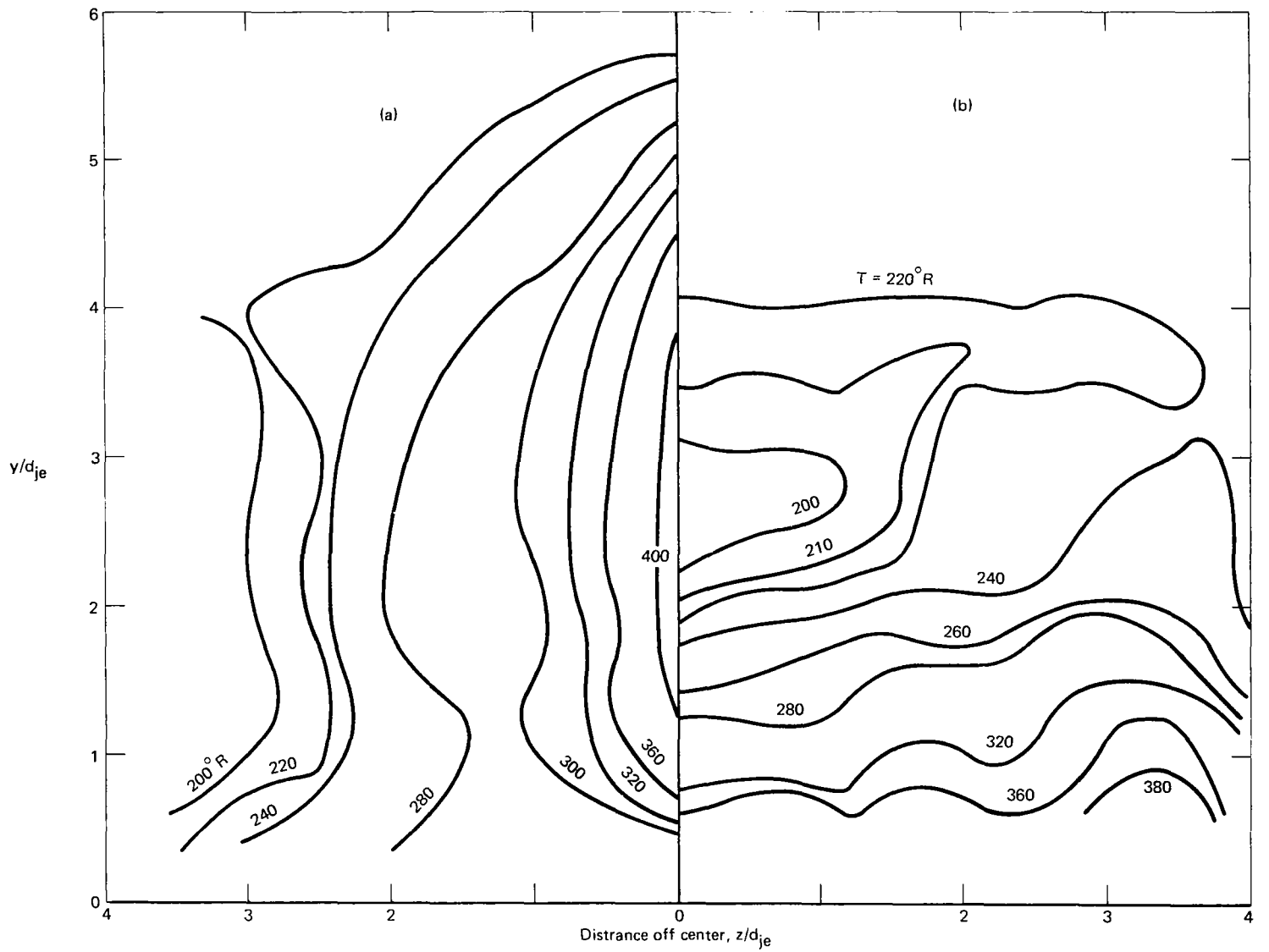

FIG. 19 DEDUCED ISOTHERMS AT $x/d_{je} = 5$ FOR FIVE–PORT INJECTOR (a) ALIGNED WITH FREESTREAM, AND (b) PERPENDICULAR TO FREESTREAM

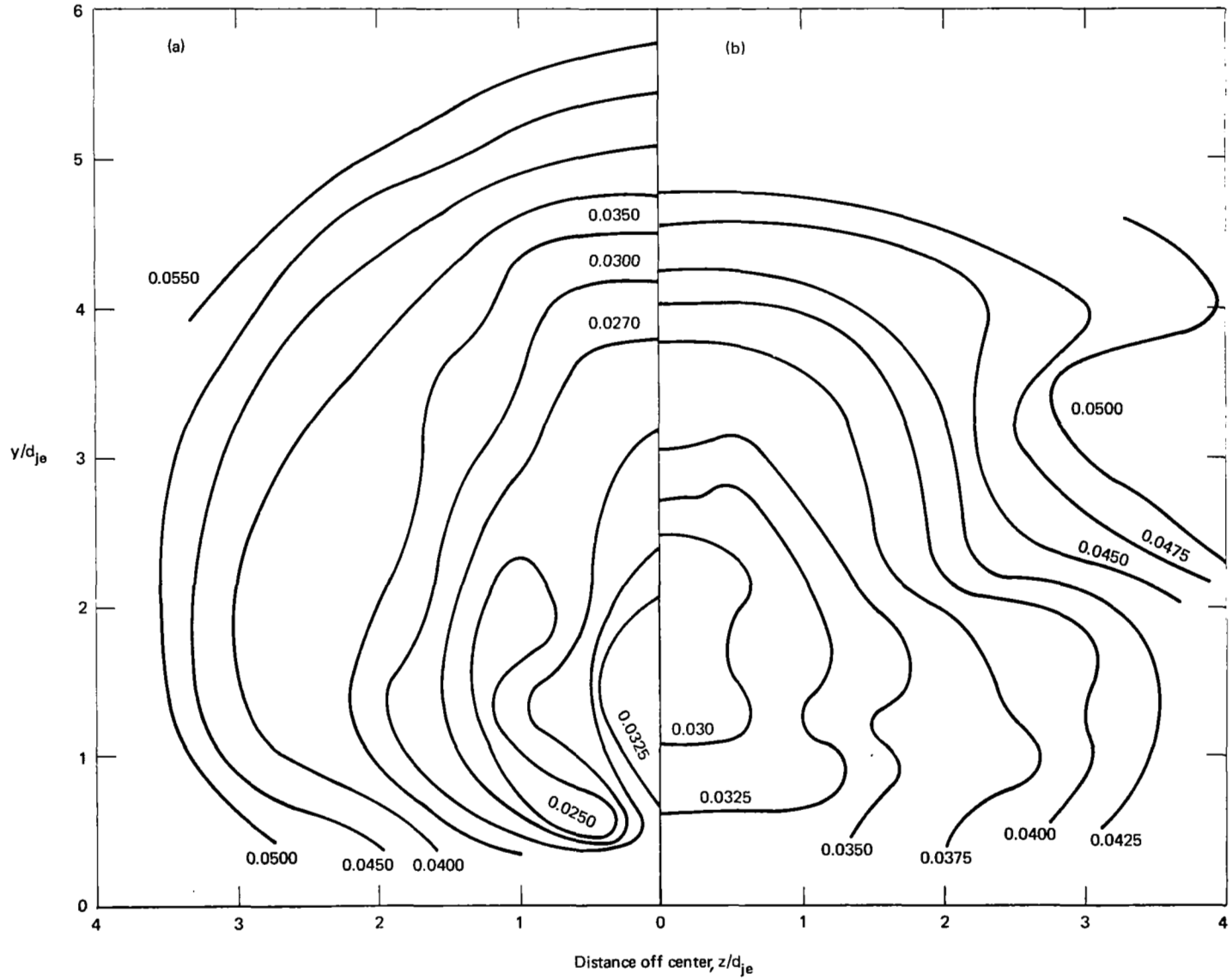

FIG. 20 DEDUCED ISOBARS AT $x/d_{je} = 5$ FOR FIVE-PORT INJECTOR AXIS (a) ALIGNED WITH FREESTREAM, AND (b) PERPENDICULAR TO FREESTREAM

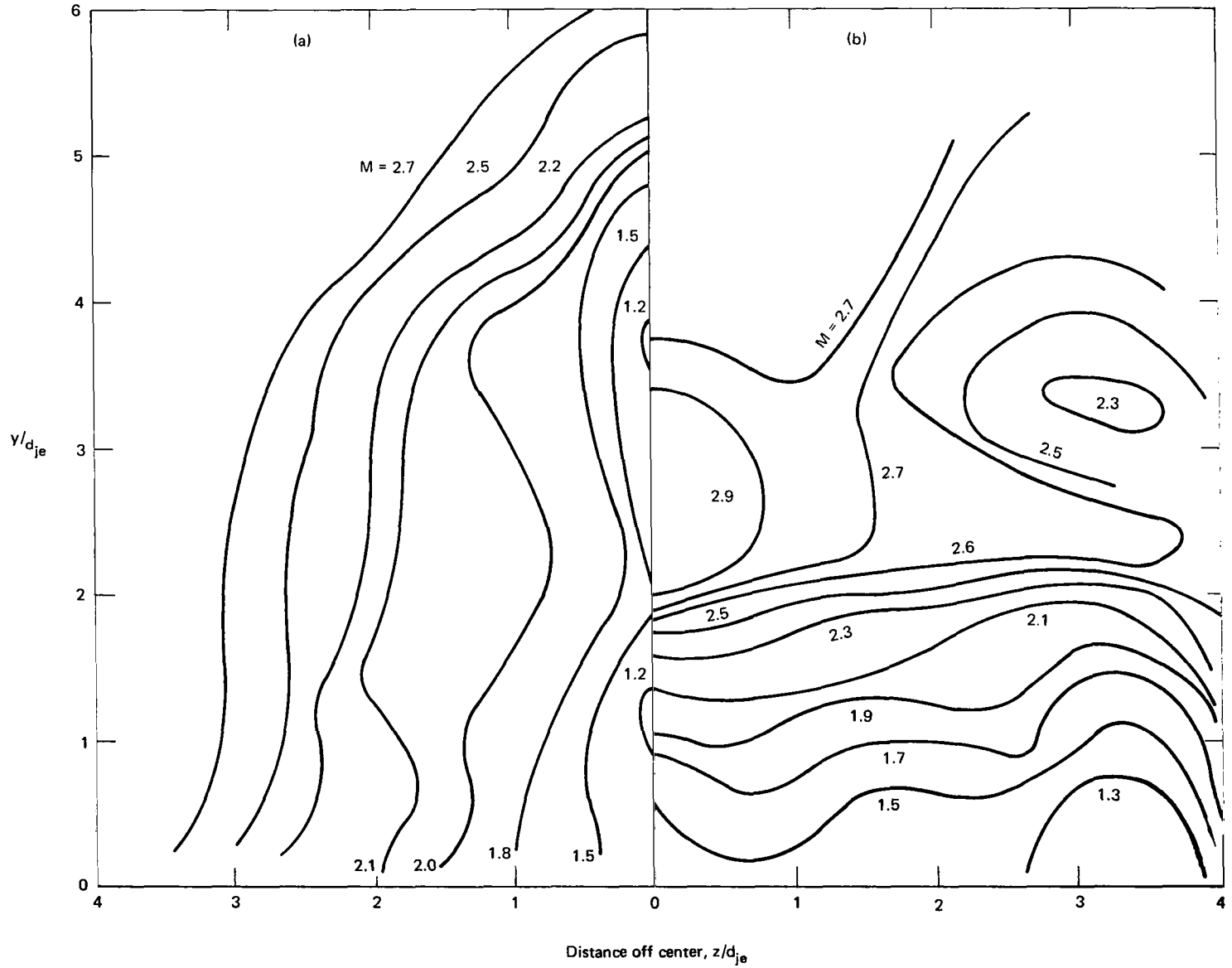

FIG. 21 DEDUCED MACH NUMBER CONTOURS FOR FIVE-PORT CIRCULAR INJECTIOR (a) ALIGNED WITH AND (b) PERPENDICULAR TO FREESTREAM.

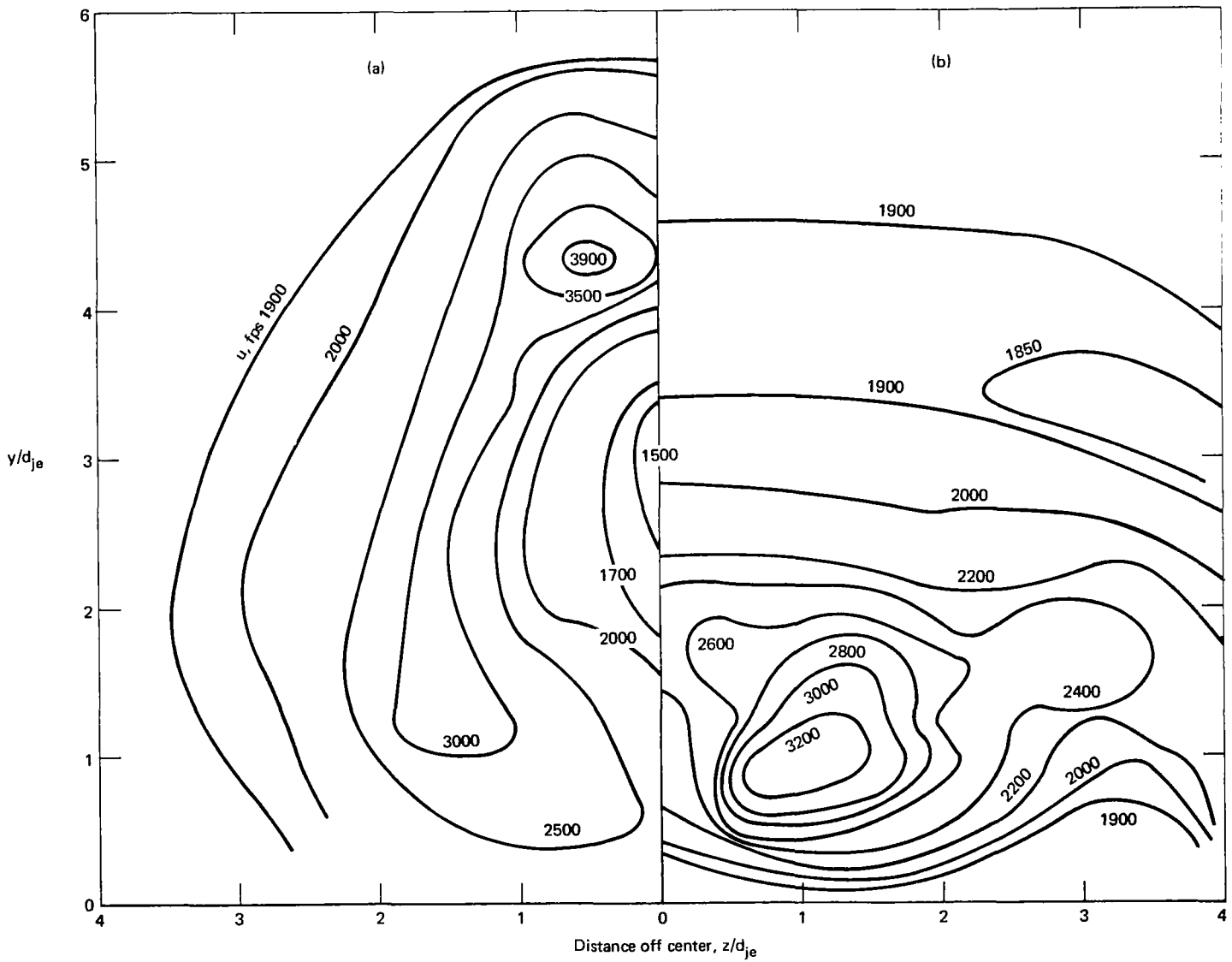

FIG. 22 DEDUCED VELOCITY CONTOURS AT $x/d_{je} = 5$ FOR FIVE-PORT INJECTOR (a) ALIGNED WITH FREESTREAM, AND (b) PERPENDICULAR TO FREESTREAM

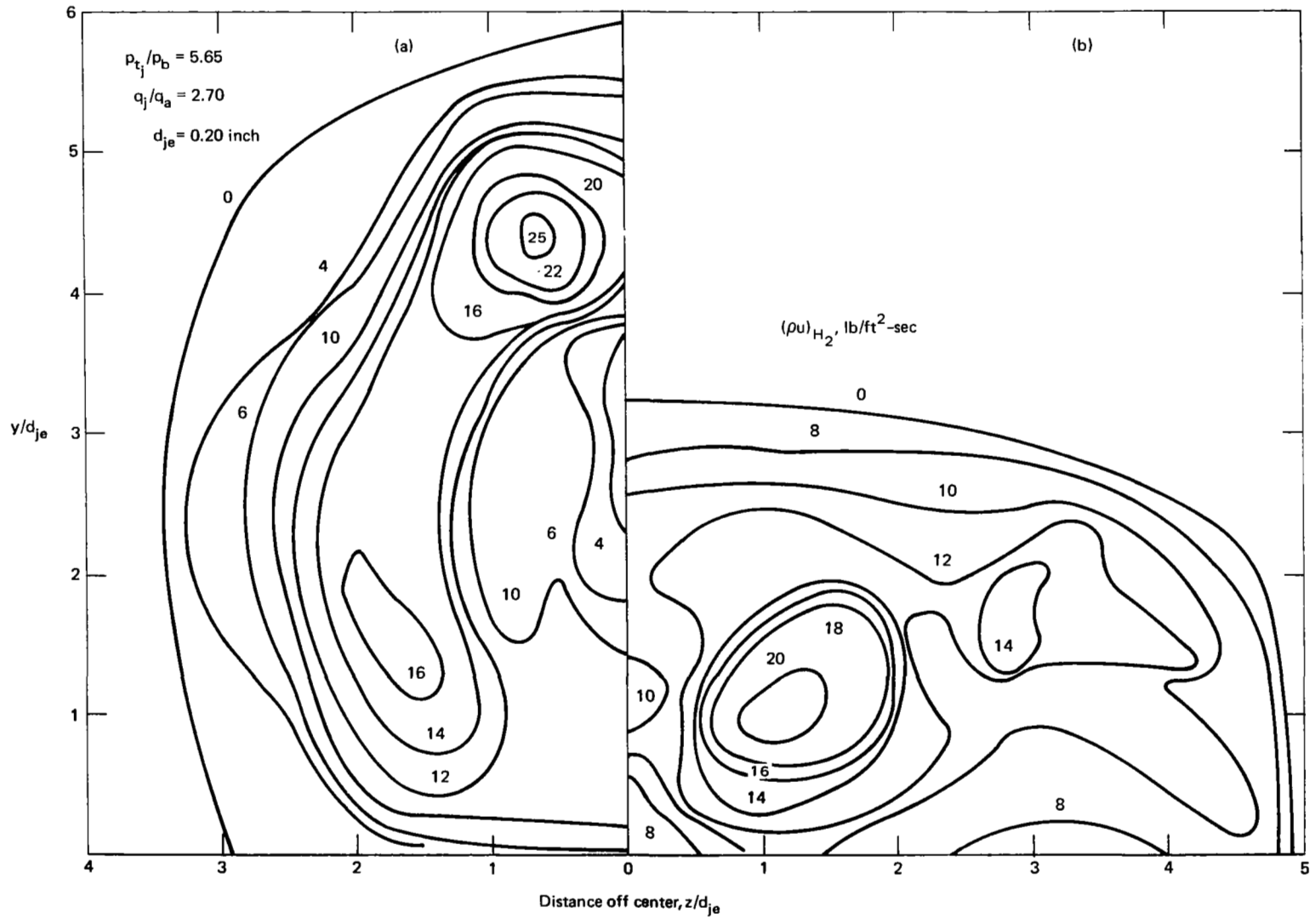

FIG. 23 HYDROGEN MASS FLUX PROFILES AT x/d_{je} = 5 FOR UNDEREXPANDED SONIC INJECTION INTO A MACH 2.7 AIRSTREAM; INJECTOR AXIS ALIGNED WITH FREESTREAM (a), AND PERPENDICULAR TO FREESTREAM (b)

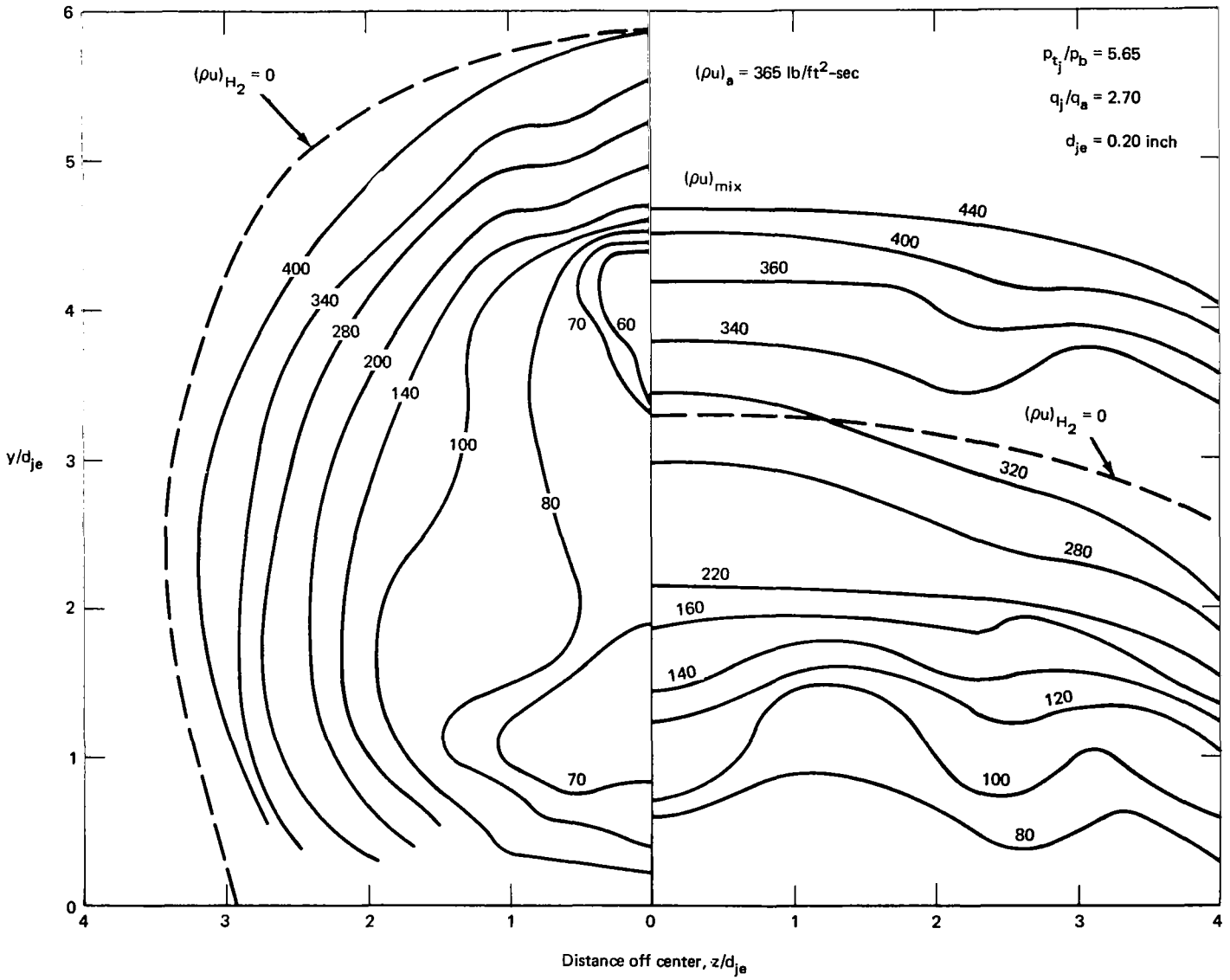

FIG. 24 DEDUCED MASS FLUX CONTOURS FOR AIR-HYDROGEN MIXTURE AT $x/d_j^* = 5$ FOR FIVE PORT INJECTOR (a) ALIGNED WITH FREESTREAM, AND (b) PERPENDICULAR TO FREESTREAM

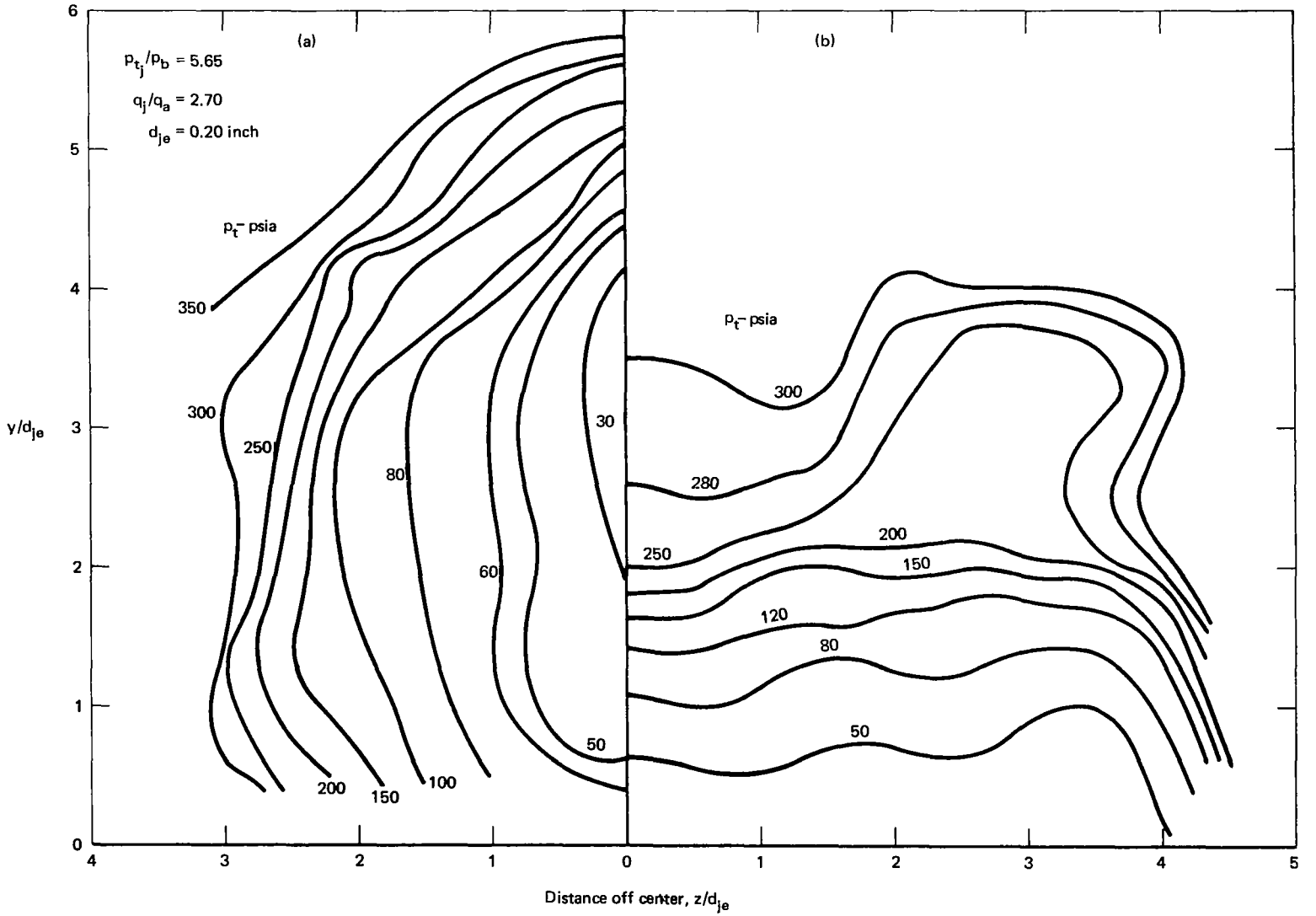

FIG. 25 DEDUCED TOTAL PRESSURE PROFILES AT x/d_{je} = 5 FOR FIVE-PORT INJECTOR (a) ALIGNED WITH FREESTREAM, AND (b) PERPENDICULAR TO FREESTREAM

NASA-Langley, 1971 — 12 CR-1794